HHS Public Access

Author manuscript

Cell Rep. Author manuscript; available in PMC 2020 August 18.

Published in final edited form as:

Cell Rep. 2020 August 04; 32(5): 107991. doi:10.1016/j.celrep.2020.107991.

Sialyl-Lewis^x Glycoantigen Is Enriched on Cells with Persistent HIV Transcription during Therapy

Florent Colomb[1,3,10], **Leila B. Giron**[1,3,10], **Leticia Kuri-Cervantes**[2,3,10], **Opeyemi S. Adeniji**[1,3,10], **Tongcui Ma**[4,5], **Harsh Dweep**[1], **Emilie Battivelli**[6], **Eric Verdin**[6], **Clovis S. Palmer**[7,8], **Hiroaki Tateno**[9], **Andrew V. Kossenkov**[1], **Nadia R. Roan**[4,5], **Michael R. Betts**[2,3], **Mohamed Abdel-Mohsen**[1,3,11,*]

[1]The Wistar Institute, Philadelphia, PA 19104, USA

[2]Department of Microbiology, Perelman School of Medicine, University of Pennsylvania, Philadelphia, PA 19104, USA

[3]Penn Center for AIDS Research (Penn CFAR), University of Pennsylvania, Philadelphia, PA 19104, USA

[4]University of California, San Francisco, San Francisco, CA 94158, USA

[5]Gladstone Institutes, San Francisco, CA 94158, USA

[6]The Buck Institute for Research on Aging, Novato, CA 94945, USA

[7]The Burnet Institute, Melbourne, VIC 3004, Australia

[8]Department of Infectious Diseases, Monash University, Melbourne, VIC 3004, Australia

[9]National Institute of Advanced Industrial Science and Technology (AIST), 1-1-1 Higashi, Tsukuba, Ibaraki 305-8566, Japan

[10]These authors contributed equally

[11]Lead Contact

SUMMARY

A comprehensive understanding of the phenotype of persistent HIV-infected cells, transcriptionally active and/or transcriptionally inactive, is imperative for developing a cure. The relevance of cell-surface glycosylation to HIV persistence has never been explored. We characterize the relationship between cell-surface glycomic signatures and persistent HIV transcription in vivo. We find that the cell surface of $CD4^+$ T cells actively transcribing HIV,

*Correspondence: mmohsen@wistar.org.

AUTHOR CONTRIBUTIONS

M.A.-M. conceived the study. F.C., L.B.G., L.K.-C., O.S.A., T.M., E.B., E.V., N.R.R., H.T., M.R.B., and M.A.-M. designed and carried out experiments. F.C., L.B.G., L.K.-C., O.S.A., T.M., H.D., C.S.P., N.R.R., H.T., A.V.K., M.R.B., and M.A.-M. analyzed and interpreted data. F.C., L.B.G., L.K.-C., O.S.A., and M.A.-M. wrote the manuscript, and all authors edited it.

SUPPLEMENTAL INFORMATION

Supplemental Information can be found online at https://doi.org/10.1016/j.celrep.2020.107991.

DECLARATION OF INTERESTS

The authors declare no competing interests.

despite suppressive therapy, harbors high levels of fucosylated carbohydrate ligands, including the cell extravasation mediator Sialyl-Lewis^X (SLe^X), compared with HIV-infected transcriptionally inactive cells. These high levels of SLe^X are induced by HIV transcription in vitro and are maintained after therapy in vivo. Cells with high-SLe^X are enriched with markers associated with HIV susceptibility, signaling pathways that drive HIV transcription, and pathways involved in leukocyte extravasation. We describe a glycomic feature of HIV-infected transcriptionally active cells that not only differentiates them from their transcriptionally inactive counterparts but also may affect their trafficking abilities.

Graphical Abstract

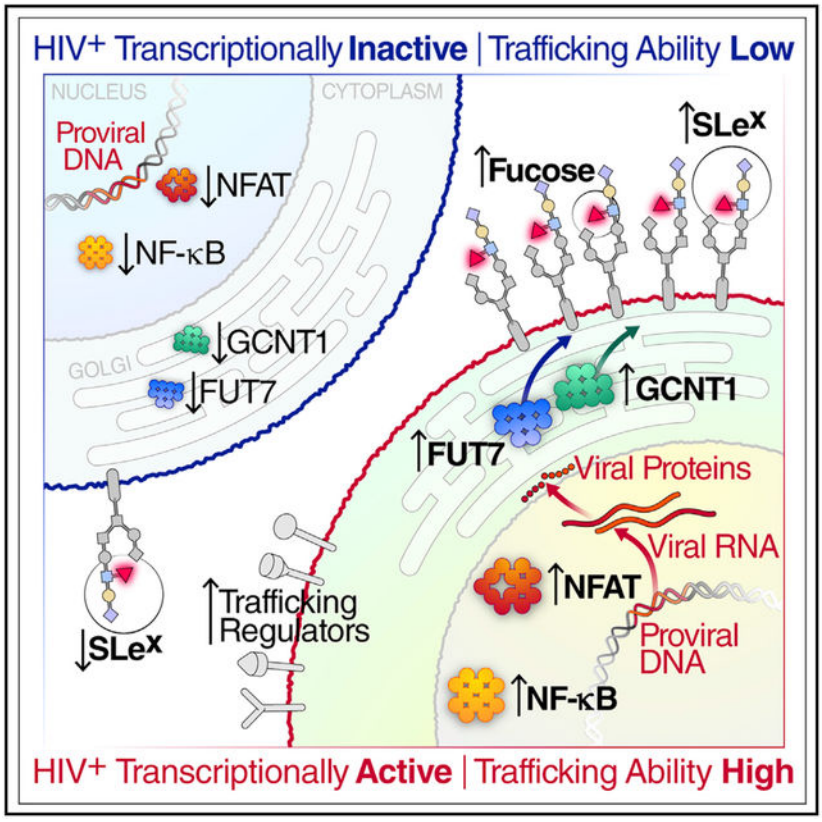

In Brief

Cell-surface glycans play a critical role in cell functions and fate. Nevertheless, the relevance of host glycosylation to HIV persistence is unknown. Colomb et al. characterized the cell-surface glycomes of HIV-infected cells during therapy and identified glycomic signatures of these cells that may affect cell trafficking and therefore HIV persistence.

INTRODUCTION

Although antiretroviral therapy (ART) has dramatically reduced morbidity and mortality for HIV-infected individuals, it does not eradicate HIV, leading to lifelong elevated immune activation and inflammation, ongoing damage to multiple organs systems, and reduction in

life expectancy (Deeks, 2011). The barrier to viral eradication during therapy is the ability of HIV to establish persistent infection mainly in $CD4^+$ T cells and possibly in other cell types in blood, as well as both lymphoid and non-lymphoid sites (Chun et al., 1997; Estes et al., 2017; Finzi et al., 1997; Wong et al., 1997). Most studies have characterized HIV latency in resting $CD4^+$ T cells, which typically do not produce viral RNA or proteins (i.e., HIV-infected transcriptionally inactive cells) (Chun et al., 1997). However, a portion of the HIV reservoir *in vivo* resides in $CD4^+$ T cells that maintain active HIV transcription, despite long-term ART (i.e., HIV-infected transcriptionally active cells) (Yukl et al., 2018). The field lacks a detailed understanding of the phenotype of persistent HIV-infected cells, transcriptionally active and/or transcriptionally inactive, that can differentiate them from uninfected cells or from each other. Such a phenotype would enable a deeper understanding of the biology of HIV persistence. Here, we describe a glycomic feature of HIV-infected transcriptionally active cells that not only differentiates them from their transcriptionally inactive counterparts but also may affect their tissue trafficking abilities and therefore HIV persistence.

All living cells assemble a diverse repertoire of glycan structures on their surface via their glycosylation machinery (Williams and Thorson, 2009). With recent advances in the fields of glycobiology and glycoimmunology (Colomb et al., 2019b), it has become clear that cell-surface glycosylation and glycan-lectin signaling play critical roles in regulating multiple cellular processes and immune functions (Barrera et al., 2002), as well as cell-cell interactions (de Freitas Junior et al., 2011) and cell-pathogen interactions (Colomb et al., 2019a; Everest-Dass et al., 2012; Giron et al., 2020b). Altered glycan structures can serve as biomarkers for cancer and infectious diseases (Giron et al., 2020a; Kuzmanov et al., 2009; Misonou et al., 2009), and they have been used to design carbohydrate-based therapeutic vaccines (Huang et al., 2013). Furthermore, several viral infections (herpes simplex virus 1 [HSV-1], varicella-zoster virus [VZV], cytomegalovirus [CMV], and human T cell leukemia virus type 1 [HTLV1]) have been shown to alter cell-surface glycosylation in infected cells (Hiraiwa et al., 2003; Kambara et al., 2002; Nyström et al., 2007, 2009). However, the relevance of the host glycosylation machinery to HIV persistence has never been explored.

We hypothesized that the cell surface of HIV-infected $CD4^+$ T cells during ART has a distinct glycomic signature that can affect their function and/or fate. To address this, we performed a comprehensive glycomic analysis of the surface of cells isolated from a primary cell model of HIV latency. We found that the cell surface of HIV-infected transcriptionally active $CD4^+$ T cells harbors high levels of fucosylated carbohydrate ligands compared with HIV-infected transcriptionally inactive cells. We confirmed these results using $CD4^+$ T cells isolated directly from HIV-infected ART-suppressed individuals. We identified that the cell extravasation mediator Sialyl-Lewis^X (SLe^X) is one of these enriched fucosylated carbohydrate ligands on the surface of HIV-infected transcriptionally active cells. We also found that active HIV transcription, but not cellular activation, induces SLe^X cell-surface expression *in vitro*. Finally, we performed a comprehensive phenotypic and transcriptomic analysis of $CD4^+$ T cells expressing high levels of SLe^X isolated from HIV-infected ART-suppressed individuals. These analyses showed that cells with high-SLe^X ($SLe^{X\text{-}Hi}$) are enriched with markers associated with HIV susceptibility, signaling pathways that drive HIV transcription, and pathways involved in leukocyte extravasation and T cell trafficking.

RESULTS

Distinct Glycomic Features of the CD4+ T Cell Surface Associate with Persistent HIV Transcription In Vitro

To examine whether $CD4^+$ T cell-surface glycomic features associate with HIV persistence, we used a dual-fluorescent, reporter-based HIV (dfHIV) that incorporates two fluorescent proteins into the HIV genome: green fluorescent protein (GFP) for monitoring HIV promoter-dependent gene expression and blue fluorescent protein (BFP) under the control of a constitutive cellular promoter. dfHIV enables the differentiation and purification of primary $CD4^+$ T cells into three populations: HIV-infected transcriptionally inactive (BFP+ GFP−) cells, HIV-infected transcriptionally active (BFP+ GFP+) cells, and uninfected (BFP − GFP−) cells (Battivelli et al., 2018; Calvanese et al., 2013; Chavez et al., 2015). Primary $CD4^+$ T cells were isolated from three HIV-negative donors, activated using αCD3/αCD28, infected with dfHIV by spinoculation, and sorted four days post-infection, yielding activated uninfected cells, infected transcriptionally inactive cells, and infected transcriptionally active cells (Figure S1A). As an additional control, we included a culture of non-activated $CD4^+$ T cells from the same donors; this culture was treated identically except that PBS was added instead of αCD3/αCD28 activating beads (Figure S1B). We isolated cell membrane proteins from each of the four populations and performed a 45-plex lectin microarray (Table S1) to profile the cell-surface glycomic signature of each population. This lectin micro- array enables sensitive analysis of multiple glycan structures by employing a panel of immobilized lectins (glycan-binding proteins) with known glycan-binding specificity, resulting in a specific glycan signature for each sample (Hirabayashi et al., 2015; Tateno et al., 2010, 2011). Using this *in vitro* latency model as a screening tool, we found that the glycomic signature of HIV-infected transcriptionally inactive cells clustered distinctly (Figures S1C and S1D) from that of the other three populations; this difference resulted from the differential binding of a set of lectins (Figure S1E), including AOL (*Aspergillus oryzae* lectin, which binds total/α1–6 core fucose), UEA-I (*Ulex europaeus* I lectin, which binds α1–2 branched fucose), ABA (*Agaricus bisporus* agglutinin lectin, which binds Thomsen-Friedenreich [TF] antigen, Galβ1–3GalNAcα1), and MAL-I (*Maackia amurensis* I lectin, which binds Siaα2–3Gal (β−1,4) GlcNAc). Our *in vitro* screening indicates that the proteins on the surface of HIV-infected transcriptionally inactive cells may have lower levels of fucose and higher levels of TF antigen and sialic acid compared with proteins on the cell-surface of the other three populations. However, as with any HIV latency model, dfHIV has limitations and caveats, including potentially poor expression of the cellular promoter, the possibility of recombination between the two reporters during reverse transcription, and the lack of the *nef* gene that is replaced by GFP (Battivelli et al., 2018; Kim et al., 2019). These caveats and others limit the utility of dfHIV to a screening tool and necessitate the *in vivo* validation of some or all of our *in vitro* preliminary observations using cells directly isolated from HIV-infected individuals on suppressive ART.

Levels of Fucosylated Carbohydrate Ligands Associate with Persistent HIV Transcription In Vivo

To validate our preliminary *in vitro* observations, we next assessed whether differential glycosylation levels corresponded with different levels of persistent HIV transcription *in*

vivo. We used fluorescently labeled versions of the lectins identified in Figure S1E (AOL, UEA-I, ABA, and MAL-I) to sort $CD4^+$ T cells from HIV-infected ART-suppressed individuals into groups with low (lowest 5% binding), medium, or high (highest 5% binding) levels of each tested glycan. Consistent with our *in vitro* data, we found that cells with low cell-surface total/core fucose, i.e., $fucose^{low}$ (lower binding to AOL), exhibited lower levels of cell-associated HIV RNA (total elongated transcripts; Yukl et al., 2018) compared with total $CD4^+$ T cells, suggesting that HIV-infected transcriptionally inactive cells *in vivo* might be depleted of cell-surface fucose. However, and unlike our *in vitro* data, in which levels of fucose were not different between activated-un-infected and activated-infected cells, we found that cells with high cell-surface total/core fucose, i.e., $fucose^{hi}$ (higher binding to AOL), exhibited higher levels of cell-associated HIV RNA compared with total $CD4^+$ T cells (Figure 1A). Comparing $fucose^{hi}$ cells to $fucose^{low}$ cells, we found that $fucose^{hi}$ cells exhibited higher levels of cell-associated HIV RNA than did $fucose^{low}$ cells (average of 17.2-fold enrichment of cell-associated HIV RNA in $fucose^{hi}$ cells compared with $fucose^{low}$ cells) despite less drastic differences in levels of HIV DNA (average of a 6.0-fold difference of HIV DNA) (Figure 1A). Furthermore, the ratio between cell-associated HIV RNA and HIV DNA (a potential marker of HIV transcriptional activity) was higher in $fucose^{hi}$ cells (average 51.2, median 41.5) than in $fucose^{low}$ cells (average 20, median 6.5) (Figure 1A).

Next, we examined binding to UEA-I (lectin that binds to branched fucose). We found that cells with high cell-surface branched fucose exhibited higher cell-associated HIV RNA compared with cells with low branched fucose (average of 8.2-fold enrichment) despite little difference in HIV DNA levels (average of 3.0-fold enrichment), but no significant difference in the ratio between cell-associated HIV RNA and HIV DNA was observed (Figure 1B). However, unlike our *in vitro* data, we did not observe any difference in cell-associated HIV RNA levels, DNA levels, or the ratio between HIV RNA and DNA in cells binding to MAL-I (Siaα2–3Gal (β−1,4) GlcNAc) or ABA lectin (TF antigen) (Figures S2A and S2B). The data in Figures 1A and 1B suggest that altered T cell-surface fucosylation patterns associate with persistent HIV transcriptional activity *in vivo*: low cell-surface fucosylation is associated with transcriptional-inactive HIV during ART, whereas high cell-surface fucosylation is associated with transcriptional-active HIV during ART.

Surface Expression of the Fucosylated Glycoantigen SLe^X on $CD4^+$ T Cells Associates with HIV Transcription In Vivo

The oligosaccharide SLe^X is a fucosylated carbohydrate that binds the selectin family of lectins and mediates many important cell-cell processes, including extravasation. Given our finding that total fucosylated glycans are enriched on the surface of HIV-infected transcriptionally active cells (Figures 1A and 1B), we hypothesized that the fucosylated glycoantigen SLe^X may be one of the fucosylated antigens enriched on these cells. SLe^X is usually attached to *O*-glycans and exists in two forms: (1) a non-sulfated form simply called SLe^X and (2) a sulfated form called CLA (cutaneous lymphocyte antigen). We used antibodies specific for SLe^X or CLA to sort $CD4^+$ T cells from HIV-infected ART-suppressed individuals. We found that cells with high cell-surface levels of SLe^X had increased cell-associated HIV RNA levels compared with cells with low-SLe^X ($SLe^{X\text{-}Low}$) expression (4.9-fold difference for cell-associated HIV RNA) despite similar levels of HIV

DNA (0.9-fold difference) (Figure 1C). The ratio between cell-associated HIV RNA and HIV DNA was higher in $SLe^{X\text{-}Hi}$ cells (average 88.0, median 46.6) compared with $SLe^{X\text{-}Low}$ cells (average 20.2, median 21.0) (Figure 1C). Similar, albeit weaker, results were observed for cells sorted using antibodies for CLA (Figure 1D). To ensure that our observations were not the result of possible latent reactivation induced by these lectins/antibodies, we treated $CD4^+$ T cells isolated from HIV-infected ART-suppressed individuals with AOL, UEA-I, SLe^X, or CLA antibodies for the same duration required to perform cell sorting (3 h). This treatment did not reactivate latent infection or induce cell-associated HIV RNA expression (Figure S2C). Altogether, these data suggest that high levels of the fucosylated glycomic antigen SLe^X on the $CD4^+$ T cell-surface associate with persistent HIV transcription *in vivo*.

We also compared levels of SLe^X and CLA on $CD4^+$ T cells (total and memory) of HIV-infected (ART-suppressed and viremic) and HIV-negative controls. We found higher frequencies of SLe^{X+} cells on total $CD4^+$ T cells of viremic (median 35%, inter-quartile range [IQR] 11.2) and ART-suppressed (median 26.8%, IQR 5.4) individuals compared with HIV-negative controls (median 15.3%, IQR 2.1). Similarly, we found a larger proportion of SLe^{X+} cells on memory $CD4^+$ T cells of viremic (median 29.7%, IQR 11.4) and ART-suppressed (median 22.6%, IQR 8.9) individuals compared with HIV-negative controls (median 15.5%, IQR 4.5) (Figure 1E). We also found a higher frequency of cells expressing CLA on total $CD4^+$ T cells of viremic (median 71%, IQR 14.2) and ART-suppressed (median 58.3%, IQR 4.4) individuals compared with HIV-negative controls (median 41.2%, IQR 6.2). A larger proportion of memory $CD4^+$ T cells similarly expressed higher levels of CLA^{high} in viremic (median 32%, IQR 10.2) and ART-suppressed (median 26.3%, IQR 5.4) individuals compared with HIV-negative controls (median 17.6%, IQR 3) (Figure 1F). We also found that levels of SLe^{X+} and CLA^+ $CD4^+$ T cells correlate with viral load in HIV-infected individuals (Figure S2D). These results indicate that high cell-surface expression of SLe^X is associated with HIV infection, irrespective of viral suppression by ART.

HIV Infection, but Not Cellular Activation, Induces the Expression of SLe^X and CLA on the Surface of Primary $CD4^+$ T Cells

To investigate whether HIV infection or cellular activation directly induces SLe^X expression, we first infected primary unstimulated $CD4^+$ T cells from three HIV-uninfected donors with either an X4 virus (IIIB) or a dual-tropic virus (89.6). Four days later, we assessed HIV infection rates and SLe^X or CLA cell-surface expression levels by flow cytometry. HIV $p24^+$ cells exhibited a higher percentage of SLe^X and CLA compared with uninfected control (Figures S3A–S3D). However, given the low levels of infection resulting from infecting $CD4^+$ T cells with HIV without prior activation, we did not observe an induction of the total percentage of SLe^{X+} or CLA^+ $CD4^+$ T cells upon infection in this experiment. Therefore, there are two potential explanations for these results: (1) HIV infection induces the expression of SLe^X and CLA on the surface of infected cells, or (2) cells expressing these markers are preferentially infected with HIV.

To test whether the first possibility is occurring, i.e., that HIV infection can directly induce the expression of SLe^X and/or CLA, we used CD44 MicroBeads to enhance HIV infection of unstimulated $CD4^+$ T cells (Terry et al., 2009). Consistent with Terry et al. (2009), CD44

MicroBeads dramatically enhanced HIV replication in unstimulated $CD4^+$ T cells with minimal impact on T cell activation (Figure S3E). Infecting primary $CD4^+$ T cells with 89.6 virus or DH12 virus (a dual-tropic virus), in the presence of CD44 MicroBeads, resulted in a significant induction of the total percentage of SLe^{X+} $CD4^+$ T cells compared with $CD4^+$ T cells treated with CD44 MicroBeads alone (Figure 2A). This induction was driven by HIV $p24^+$ cells (Figure 2A). Next, we examined the impact of HIV infection on CLA expression. Given the high background of CLA on primary $CD4^+$ T cells (Figure S3D), we first depleted CLA^+ $CD4^+$ T cells using rat anti-human CLA antibody coupled with anti-rat kappa MicroBeads to remove background and improve the chance of observing an increase in the total percentage of CLA^+ $CD4^+$ T cells upon infection (Figure S3F shows the successful depletion of CLA from the surface of primary $CD4^+$ T cells). Infecting CLA-depleted primary $CD4^+$ T cells with 89.6 or DH12 viruses, in the presence of CD44 MicroBeads, resulted in a significant induction of the total percentage of CLA^+ $CD4^+$ T cells compared with $CD4^+$ T cells treated with the CD44 MicroBeads alone (Figure 2B). This induction was significantly more pronounced in HIV $p24^+$ cells than in $p24^-$ cells (Figure 2B). Potential explanations for the induction of CLA in $p24^-$ cells are that some of these cells are infected but with insufficient p24 expression to be detected by flow cytometry or that there is transcellular transactivation by viral proteins. Importantly, infection with heat-inactivated virus was unable to induce CLA, suggesting that active viral replication is needed for HIV-mediated CLA induction (Figure S3G).

To examine whether HIV infection induces the expression of glycosyltransferases (enzymes that catalyze glycosidic bond formation) involved in the production of SLe^X and CLA, we infected H9 cells (HIV-susceptible human $CD4^+$ T cell line) with either 89.6 or NL4–3 viruses and examined the protein expression of some of these glycosyltransferases (Figure 2C). In particular, we exam ined the protein expression of FUT7 and FUT6 (α-(1,3)-fucosyltransferases), enzymes that add α-(1,3)-fucose to the SLe^X or CLA carbohydrate structures, and B4GALT5, (β−1,4-galactosyltransferase 5), an enzyme that adds galactose into the *O*-glycan backbone of SLe^X and CLA (Figure 2C). We also tested for HIV p24 protein expression as a marker of successful HIV infection. As shown in Figure 2C, HIV infection induced the protein expression of these glycosyltransferases involved in SLe^X and CLA production. Altogether, these results demonstrate that HIV infection can directly induce the expression of SLe^X and CLA on primary $CD4^+$ T cells; however, it does not exclude the additional possibility that cells constitutively expressing these markers are preferentially infected with HIV.

We also activated primary $CD4^+$ T cells from three HIV-uninfected donors with five activating agents (αCD3/αCD28, tumor necrosis factor alpha [TNF-α], interleukin-2 [IL-2], IL-2+αCD3/αCD28, or IL-2+TNF-α) for four days and measured SLe^X and CLA expression. As shown in Figure S6H, we did not observe induction of SLe^X or CLA under these activation conditions. These results suggest that HIV infection directly induces the cell-surface expression of SLe^X and CLA but cellular activation (using the aforementioned conditions) does not.

SLe^X Expression Is Enriched on Central Memory and Naive CD4$^+$ T Cells and Associates with Higher Activation Status

To examine the composition and distribution of SLe^X expression in CD4$^+$ T cell subsets, T cells were obtained from peripheral blood mononuclear cell (PBMC) samples of uninfected, ART-suppressed, and viremic HIV-infected donors. Flow cytometry gating strategies used for identifying the CD4$^+$ T cell subsets and SLe^X expression and representative examples are shown in Figure S4A. We found that the T cell memory subset distribution within SLe^{X+}-expressing cells was similar between HIV-negative and HIV-infected individuals, and most SLe^{X+} cells had either a naive or a central memory T cell (T_{CM}) phenotype (Figure 3A). Naive, stem memory T cells (T_{SCM}), T_{CM}, and transitional memory T cells (T_{TM}) from ART-suppressed individuals had higher frequencies of SLe^{X+} cells compared with their counterparts from HIV-negative controls (Figure 3B). All CD4$^+$ T cell subsets exhibit elevated SLe^X in viremic individuals (Figure 3B). We also examined the expression of 17 cell-surface markers measured on SLe^{X+} and SLe^{X-} CD4$^+$ T cells and found that SLe^{X+} CD4$^+$ T cells from HIV-infected ART-suppressed individuals had higher proportions of the HIV co-receptors CCR5 and CXCR4, as well as CCR7, CD25, CD27, CD38, CD45RA, CD127, FoxP3, and Ki-67. In contrast, the levels of CD95 were lower in SLe^{X+} compared with SLe^{X-} CD4$^+$ T cells (Figure 3C; Figure S5). Using these markers, we identified the T helper (Th) phenotype of SLe^{X+} CD4$^+$ T cells. We analyzed the frequency of circulating follicular T cells ([cTfhs] CXCR5$^+$ PD1$^+$), regulatory T cells ([Tregs] non-cTfhs CD127$^{lo/-}$ CD25$^+$ FoxP3$^+$), Th1 (non-cTfhs/non-Tregs CXCR3$^+$ CCR4$^-$ CCR6$^-$), Th2 (non-cTfhs/non-Tregs CXCR3$^-$ CCR4$^+$ CCR6$^-$), Th17 (non-cTfhs/non-Tregs CXCR3$^-$ CCR4$^+$ CCR6$^+$), and Th17+1 (non-cTfhs/non-Tregs CXCR3$^+$ CCR4$^-$ CCR6$^+$) within these cells (Figure S6A). We found that SLe^{X+} CD4$^+$ T cells are mainly of the Th2, Th17, and CXCR5$^+$ non-cTfh phenotypes, irrespective of HIV/ART status (Figure S6B). We also found that the frequency of cTfhs, CXCR5$^+$, Th17 cells, and Th2 cells expressing SLe^{X+} was higher in viremic individuals compared with HIV-negative controls. Furthermore, the frequency of CXCR5+ non-cTfhs, Th17 cells, and Th2 cells expressing SLe^{X+} was higher in ART-suppressed individuals compared with HIV-negative controls (Figure S6C). Altogether, these data show that most SLe^{X+} CD4$^+$ T cells are of the naive and T_{CM} phenotypes, express markers associated with HIV susceptibility, and express one or more activation markers.

CLA^{high} CD4$^+$ T Cells Cluster Distinctly from CLA^{low} and CLA^{negative} CD4$^+$ T Cells

Next, we examined the composition and distribution of CLA$^+$ cells within CD4$^+$ T cell subpopulations. Flow cytometry gating strategies used for identifying CD4$^+$ T cell subsets, and representative examples of CLA expression are shown in Figure S4B. We performed unbiased clustering and principal-component analyses (PCAs) using the expression of 17 cell-surface markers measured on CLA^{high}, CLA^{low}, and CLA^{negative} CD4$^+$ T cells (Figure 4A). These analyses showed that CLA^{high} cells have a phenotype distinct from CLA^{low} and CLA^{negative} CD4$^+$ T cells, and this phenotype is similar between viremic and aviremic HIV-infected individuals (Figure 4A). Of note, HIV and ART status did not cluster separately across CLA^{negative}, CLA^{low}, and CLA^{high} subpopulations. We found that CLA^{high} cells have almost exclusively a T_{CM} phenotype (Figure 4B). We also found that their frequency is elevated in HIV-infected individuals regardless of treatment status (Figure 4C) and that they are enriched with HIV co-receptors and activation markers (Figure 4D). Focusing on Th

phenotypes, we found that CLA^{high} CD4^{+} T cells are mainly of Th2 and Th17 phenotypes, irrespective of HIV/ART status (Figure S6C). We also found that the frequency of cTfhs, Tregs, CXCR5^{+}, Th1, and Th17 cells expressing CLA^{high} was higher in viremic individuals compared with HIV-negative controls. Furthermore, the frequency of CXCR5^{+} non-cTfhs and Th17+1 cells expressing CLA^{high} was higher in ART-suppressed individuals compared with HIV-negative controls (Figure S6D). Altogether, these data show that CLA^{high} CD4^{+} T cells have a T_{CM} phenotype and exhibit a distinct phenotype compared with CLA^{low} and CLA^{negative} CD4^{+} T cells.

SLe^{X+} CD4^{+} T Cells Are Enriched with Several Host Proteins Known to Be Associated with HIV Persistence during ART

Some persistence-associated host proteins are enriched in HIV-infected cells during ART, including PD-1, TIGIT, CTLA-4, CCR6, Survivin, and CD30 (Fromentin et al., 2016; Gosselin et al., 2017; Hogan et al., 2018; Kuo et al., 2018; McGary et al., 2017). The expression patterns of these factors in the context of transcriptionally active versus transcriptionally inactive cells are not clear, except for CD30, which is known to be enriched on the surface of cells actively transcribing HIV (Hogan et al., 2018). We examined the relationship between SLe^{X} expression and PD-1, TIGIT, CTLA-4, CCR6, CD30, and Survivin expression on freshly isolated peripheral blood CD4^{+} T cells from nine HIV-infected ART-suppressed individuals by CyTOF (cytometry by time of flight). We found that relative to SLe^{X-} cells, SLe^{X+} cells were enriched for cells expressing PD-1, TIGIT, CTLA-4, CCR6, and CD30. In comparison, SLe^{X-} cells are enriched for cells expressing Survivin (Figure 5A). Consistently, CD4^{+} T cells expressing high levels of PD-1, TIGIT, CTLA-4, CCR6, and CD30 express higher levels of SLe^{X} compared with cells that do not express these markers. In contrast, Survivin^{+} cells express low levels of SLe^{X} compared with survivin^{-} cells (Figure 5B). These results suggest that SLe^{X} expression is associated with the expression of several putative markers of HIV persistence on the surface of CD4^{+} T cells during suppressive ART.

SLe^{X+} CD4^{+} T Cells Are Enriched for Pathways Involved in T Cell Extravasation and HIV Transcription

Using RNA sequencing (RNA-seq), we characterized the transcriptomes of SLe^{X-Hi} and SLe^{X-Low} CD4^{+} T cells isolated from four HIV-infected ART-suppressed individuals. We first examined the gene expression patterns of some glycosyltransferases involved in the synthesis of mature, core 2 *O*-glycans bearing SLe^{X}. As expected, SLe^{X-Hi} cells express high levels of GCNT1 (β−1,3-galactosyl-O-glycosyl-glycoprotein β−1,6-N-acetylgluco saminyltransferase) and FUT7 (Figure 6A). GCNT1 is a core 2 *O*-glycan initiation enzyme essential to the formation of Gal β1–3(GlcNAc β1–6)GalNAc structures and the core 2 *O*-glycan branch. These data confirm that SLe^{X} is enriched on the sorted populations used in the RNA-seq experiments.

Overall, we found 1,086 genes significantly differentially expressed (false discovery rate [FDR] < 5%, at least 2-fold) between SLe^{X-Hi} and SLe^{X-Low} CD4^{+} T cells. We used Ingenuity Pathway Analysis (IPA) to evaluate the functional significance of the genes. IPA identified clear enrichment of pathways and functions (Figures 6B–6D) associated with

higher leukocyte migration and extravasation in $SLe^{X\text{-}Hi}$ (cells harboring more transcriptionally active HIV) compared with $SLe^{X\text{-}Low}$ cells (cells harboring more transcriptionally inactive HIV). We found that two signaling pathways known to drive HIV transcription were enriched in $SLe^{X\text{-}Hi}$ versus $SLe^{X\text{-}Low}$ $CD4^+$ T cells. These signaling pathways are nuclear factor κB (NF-κB) (Chan and Greene, 2011; Mbonye and Karn, 2014) and NFAT (Bosque and Planelles, 2009; Mbonye and Karn, 2014) (Figures 6B, 6C, and 6E). These data suggest that the NF-κB and/or NFAT signaling pathways may underlie the higher persistent HIV transcription in $SLe^{X\text{-}Hi}$ compared with $SLe^{X\text{-}Low}$ cells.

DISCUSSION

In this study, we examined the relationship between cell-surface glycosylation patterns of HIV-infected cells and persistent HIV transcription. We identified fucosylated carbohydrates to be enriched on the surface of HIV-infected transcriptionally active cells despite ART suppression. Conversely, the levels of these fucosylated carbohydrates are low on the surface of HIV-infected transcriptionally inactive cells. This glycomic feature of HIV-infected cells actively producing HIV transcripts is possibly a product of viral transcription and potentially has a phenotype significance on the trafficking abilities of these cells. In particular, the cell extravasation mediator SLe^X is one of the fucosylated carbohydrate ligands enriched on the surface of HIV-infected transcriptionally active cells and reduced on the surface of HIV-infected transcriptionally inactive cells. This observation would suggest potential differential trafficking abilities of these cells. Such differential abilities might affect maintenance of HIV persistence and should be considered when targeting HIV reservoirs in blood and tissues.

Identifying host factors enriched in HIV-infected cells (both latent and actively transcribing) during ART could provide the HIV cure field with vital biological clues into the molecular pathways involved in viral persistence. These host factors may be different between HIV-infected transcriptionally active and HIV-infected transcriptionally inactive cells. For example, it has been observed that persistent HIV proviruses are enriched in several memory $CD4^+$ T cell compartments (Chomont et al., 2009). Some host factors are also enriched in HIV-infected cells (transcriptionally active or not) during long-term ART. These factors include the immune negative checkpoints PD-1, TIGIT, LAG-3 (Fromentin et al., 2016), and CTLA-4 (McGary et al., 2017), as well as other factors such as CD2 (Iglesias-Ussel et al., 2013), CCR6 (Gosselin et al., 2017), and Survivin (Kuo et al., 2018). Other host factors are shown to be enriched, in particular, in HIV-infected transcriptionally active cells, such as CD30 (Hogan et al., 2018) and CD20 (Serra-Peinado et al., 2019). These factors, especially those that reside on the cell surface, may be useful for targeting these cells and can provide a better understanding of HIV persistence biology.

Recent advances in the cancer field demonstrated that the aberrant glycosylation pattern of cancer cells alters their functions and interaction with the immune system (Pinho and Reis, 2015; Rodríguez et al., 2018). Such advances have promoted increasing interest in developing novel tools to target the tumor glycocode (Rodríguez et al., 2018). However, the relevance of the host glycosylation machinery to HIV persistence has not been evaluated previously. We found that cell-surface fucosylation is enriched on the surface of HIV-infected transcriptionally active cells and is reduced on the surface of HIV-infected

transcriptionally inactive cells *in vitro*. Future studies will be needed to identify the potential additive enrichment of persistent HIV-infected cells when combining cell-surface fucosylation with other host factors, mentioned earlier, that are enriched on HIV-infected cells during ART. Most proviruses persisting in HIV-infected ART-treated individuals harbor mutations and/or deletions, rendering them defective (Bruner et al., 2016; Ho et al., 2013). However, not all intact viruses are inducible, and both intact and defective proviruses can express viral RNA and proteins (Imamichi et al., 2020; Pollack et al., 2017). It is possible that cells with high cell-surface fucose in general (and SLe^X in particular) are enriched with intact HIV genomes compared with cells with low cell-surface fucose, given the higher HIV transcriptional ac tivity of these former cells. However, this possibility will need to be investigated using single-genome, near-full-length proviral sequencing to determine the genetic makeup of the virus infecting cells with differential levels of fucosylation.

Many T cell processes and functions are shaped by cell-surface glycosylation (Pereira et al., 2018). For example, T cell-surface fucosylation is critical for T cell activation via T cell receptor (TCR) signaling (Liang et al., 2018), and the fucosylation of T cell immune negative checkpoints (such as PD-1) is critical for their function (Okada et al., 2017). It is unclear how these two published observations may contribute to our findings. Among the total fucosylated carbohydrate ligands, we found that SLe^X, which has important implications for T cell trafficking, is enriched on the surface of HIV-infected transcriptionally active cells. However, this 5-fold enrichment is significantly lower than the enrichment of total/core fucose (17-fold) found when using AOL (which binds total/core fucose). These results suggest that other fucosylated ligands may be enriched on the surface of HIV-infected transcriptionally active cells and depleted on the surface of HIV-infected transcriptionally inactive cells. Identifying these other glycan structures and their exact protein and lipid backbones should be the subject of future studies and will likely allow us a better understanding of the role of cell-surface fucosylation in modulating T cell functions and HIV persistence. Further studies will also be needed to examine the potential biological significance of this altered fucosylation on HIV-infected T cell biology and function.

The process of leukocyte extravasation is well described and requires binding of selectins (a type of lectins) to fucosylated carbohydrates. T cells exit the vasculature to reach their target tissue through the leukocyte adhesion cascade, a coordinated series of events involving (1) selectin-mediated rolling, (2) chemokine-triggered activation, and (3) integrin-dependent arrest (Ley et al., 2007). Selectins are a family of receptors comprising platelet (P), endothelial (E), and leukocyte (L) selectin. To mediate rolling, selectins bind with their fucosylated carbohydrate ligands, notably SLe^X (Impellizzeri and Cuzzocrea, 2014). Upon antigen stimulation, some T cells become activated and induce cell-surface expression of SLe^X; SLe^X binding to P- and E-selectin on vascular endothelium regulates the trafficking of these T cells into various non-lymphoid tissues. Some of these T cells can traffic back to the lymph nodes through the lymph (Haddad et al., 2003; Wolber et al., 1998; Xie et al., 1999). Our transcriptomic analysis demonstrated enrichment of T cell extravasation and trafficking pathways in $CD4^+$ T cells with high levels of SLe^X compared with cells with low levels of SLe^X. These data suggest that HIV-infected transcriptionally active $CD4^+$ T cells may have higher trafficking abilities compared with HIV-infected transcriptionally inactive $CD4^+$ T cells. These differential characteristics of HIV-infected T cells trafficking to

lymphoid and non-lymphoid tissues in their HIV transcriptional activity and cell-surface glycomic features could be considered for targeting the tissue-based HIV reservoir. Selectin antagonists such as bimosiamose (Friedrich et al., 2006; Kirsten et al., 2011; Mayr et al., 2008) and rivipansel (Telen et al., 2015) have been used in humans and could be explored in the context of HIV infection to temporarily trap HIV-infected cells in blood for immunotherapeutic clearance.

Our data suggest that HIV infection can directly induce the expression of SLe^X on the surface of $CD4^+$ T cells. The mechanism that underlies this induction is not clear. Different viral infections have been described to induce the cell-surface expression of fucosylated carbohydrate ligands, including HSV-1, VZV, and CMV (Nyström et al., 2007, 2009). HTLV1 infection has been shown to induce SLe^X through the viral transactivator *Tax* (Hiraiwa et al., 2003; Kambara et al., 2002; Umehara et al., 1996). Future studies will be needed to investigate the possibility that HIV induces SLe^X through its viral transactivator *Tat*. However, infection cannot explain the entirety of the difference we found in the levels of SLe^X on the surface of $CD4^+$ T cells from viremic and ART-suppressed HIV-infected individuals, because not all T cells from HIV-infected individuals are infected. There are two possibilities: (1) Although our data show that activation using αCD3/αCD28, TNF-α, or IL-2 does not induce the expression of SLe^X, we cannot exclude the possibility that stimulation using other stimulants, *in vivo*, would induce SLe^X expression. (2) Viral proteins (including *tat* and *nef*) can exist in circulation (especially in exosomes) and can be taken by uninfected cells and affect them. HTLV-1 *Tax* significantly enhances the ability of cell activation to induce FUT7 (Hiraiwa et al., 1997). Therefore, although our data show that active HIV infection can directly induce SLe^X, likely other factors synergize with HIV infection, leading to this enrichment *in vivo*. Although our data show that HIV infection can directly induce the expression of SLe^X, it does not exclude the possibility that cells are preferentially infected with HIV. This latter possibility is supported by our observation that cells expressing SLe^X are enriched with HIV co-receptors and activation markers. Future studies will be needed to determine the contribution of (1) the direct impact of HIV transcription on SLe^X expression and (2) the impact of cellular susceptibility to infection on our observed enrichment of SLe^X on the surface of HIV-infected transcriptionally active cells during ART. In addition, several cancers have higher levels of fucose in general (Agrawal et al., 2017; Blanas et al., 2018), and SLe^X in particular (Julien et al., 2011; Nakamori et al., 1997; Trinchera et al., 2017), that affect their functions and contribute to their metastasis (through binding to selectins). Therefore, several mechanisms clearly contribute to SLe^X induction. Understanding the upstream modulator or modulators of fucose and SLe^X enrichment on HIV-infected transcriptionally active cells, as well as the downstream consequences of this enrichment, should be the subject of future studies to better understand HIV persistence.

Our study provides the first insight into a potential role of circulating $CD4^+$ T cell-surface glycome in persistent HIV transcription activity. However, our findings have limitations, including the following: (1) Our data were obtained from blood; there is a need to analyze the potential enrichment of fucosylated glycans, including SLe^X, in tissues such as lymph nodes and gut-associated lymphoid tissues. (2) Our *in vivo* phenotyping analysis was done mainly on cryopreserved PBMCs, and it is possible that freezing/thawing affects these

phenotypes. (3) Our data were obtained using cross-sectional samples from chronically infected adults; there will be a need to analyze longitudinal changes, acute infection, and samples from geographically and/or age-distributed cohorts. (4) We did not comprehensively validate *in vivo* all glycomic signatures of HIV-infected cells identified in *in vitro*. Future studies will need to examine whether additional glycomic signatures of HIV-infected cells can be confirmed *in vivo* or identified *in vitro* (using other HIV latency models and/or other glycomic technologies such as mass spectrophotometry). That said, we think our study is an important step toward elucidating the potential glycomic underpinnings of HIV persistence. In summary, we identified fucosylation to be a feature of persistent HIV transcriptional activity *in vivo*. The role of cell-surface fucosylation (including SLe^X expression) in HIV persistence warrants further investigation to better understand persistent HIV expression during ART and identify glycan-based interactions that can be targeted for novel HIV immunotherapies.

STAR★METHODS

RESOURCE AVAILABILITY

Lead Contact—Further information and requests for resources and reagents should be directed to and will be fulfilled by the Lead Contact, Mohamed Abdel-Mohsen (mmohsen@wistar.org).

Materials Availability—This study did not generate new unique reagents.

Data and Code Availability—The RNA-seq data were submitted to GEO (https://www.ncbi.nlm.nih.gov/geo/) under accession number GSE151453

EXPERIMENTAL MODEL AND SUBJECT DETAILS

Cell lines—ACH-2, H9, and TZM-bl cells were maintained at 37°C in RPMI 1640 medium supplemented with 10% FBS, L-glutamine (2 mM), penicillin (50 U/ml), and streptomycin (50 mg/ml).

Human primary $CD4^+$ T Cell—We used $CD4^+$ T cells isolated from the peripheral blood mononuclear cell (PBMC) of 11 HIV-infected ART-suppressed individuals for the sorting experiments in Figures 1A–1D (Table S2). Frozen PBMCs of these individuals were obtained from 1) the External Quality Assurance Program Oversight Laboratory (EQAPOL), located at the Duke Human Vaccine Institute's Immunology and Virology Quality; and 2) The Wistar Institute and the Philadelphia FIGHT cohort. Frozen PBMCs from HIV-negative, HIV-infected ART-suppressed, and HIV-infected viremic individuals were used for the flow cytometry profiling experiments in Figures 1E, 1F, 3, and 4 (Table S3). PBMCs from HIV-infected viremic and ART-treated individuals were obtained from INER-CIENI (Mexico). Healthy HIV-negative PBMC samples were obtained from the University of Pennsylvania Human Immunology Core. We used freshly isolated $CD4^+$ T cells from the PBMC of nine HIV-infected ART-suppressed individuals for the CyTOF experiments in Figure 5 (Table S4). PBMCs of these individuals were obtained from The Wistar Institute and the Philadelphia FIGHT cohort. Research protocols were approved by Duke University, The

Wistar Institute, Philadelphia FIGHT, and the University of Pennsylvania Committees on Human Research. Written informed consent was obtained, and all data and specimens were coded to protect confidentiality.

METHOD DETAILS

Primary CD4$^+$ T cells infection with the dual fluorescent reporter-based HIV (dfHIV)—Primary CD4$^+$ T cells were isolated from the PBMCs of three HIV-uninfected donors using the Human EasySep Human CD4+ T Cell Isolation Kit (StemCell Technologies, cat# 17952). Purified CD4$^+$ T cells were cultured in RPMI 1640 medium supplemented with 10% fetal bovine serum (FBS), L-glutamine (2 mM), penicillin (50 U/ml), and streptomycin (50 mg/ml). Purified CD4$^+$ T cells were stimulated with αCD3/αCD28 activating beads (Life Technologies, cat 11131D) at a concentration of 1 bead/cell in the presence of 30 U/ml IL-2 (PeproTech, cat# 200–20) for three days. Non-Activated CD4$^+$ T cells from the same donors were included as controls; this culture was treated identically except PBS was added instead of activating beads. Cells were then spinoculated with either PBS or dfHIV (generously provided to us by Dr. Leonard Chavez at Vitalant Research Institute) (Battivelli et al., 2018; Calvanese et al., 2013; Chavez et al., 2015), at a concentration of 100 ng of p24 per 1×10^6 cells for 2 h at 1,200 × g at 37°C. After spinoculation, all cells were returned to culture in the presence of 30 U/ml IL-2. Cells were sorted four days post-infection based on GFP and BFP fluorescence using BD FACSAria II (BD Biosciences). Cell-surface molecules from at least 100,000 sorted cells of each of the four populations were purified and labeled using ProteoExtract Subcellular Proteome Extraction Kit (Merck, cat# 539790).

Glycomic analysis using lectin microarrays—A lectin microarray platform was used to profile 45 different glycan structures on the surface of sorted cells (Hirabayashi et al., 2013, 2015; Nagahara et al., 2008; Tateno et al., 2007, 2009, 2010, 2011; Uchiyama et al., 2008). The lectin array employs a representative panel of immobilized lectins with known glycan structure binding specificity. Cell-membrane proteins were labeled with Cy3 dye (GE Healthcare, cat# GEPA23001) and hybridized to the lectin microarray. The resulting lectin chips were scanned for fluorescence intensity on each lectin-coated spot using an evanescent-field fluorescence scanner (GlycoTechnica Ltd.). All samples were run in triplicate, and the average of the triplicate was used for analysis. Data were normalized using the global normalization method.

Sorting primary CD4$^+$ T cells based on their binding to AOL lectin, UEAI lectin, SLe^X antibody, or CLA antibody—Primary CD4$^+$ T cells were negatively isolated from PBMCs of HIV-infected ART-suppressed individuals using the Human EasySep Human CD4$^+$ T Cell Isolation Kit (StemCell Technologies, cat#17952). Cells were stained with AOL-biotin conjugated (TCI America, cat# A26591ML) followed with Streptavidin-APC (Biolegend, cat# 405207), UEA-I FITC (Vector labs, cat# FL-1061–2), SLe^X (CSLEX1, AF647; BD biosciences, cat# 563526), or CLA (HECA-452, AF647; Biolegend, cat# 321309). Cells were then sorted using the MoFlo Astrios EQ, Cell Sorter (Beckman Coulter) into cells with the lowest 5% binding, highest 5% binding, and rest of the cells.

Cellular DNA and RNA extraction—Sorted cells were lysed in RLT Plus Buffer (Allprep isolation kit, QIAGEN, cat# 80224). Total DNA and total RNA were extracted simultaneously from the lysates using the Allprep DNA/RNA/miRNA Universal Kit (QIAGEN, cat# 80224) with on-column DNase treatment (QIAGEN, cat# 79254). RNA samples were quantified using Qubit 2.0 Fluorometer (Life Technologies), and RNA integrity was checked with 2100 Bioanalyzer (Agilent Technologies).

qPCR quantification of HIV DNA and cell-associated HIV RNA—Total HIV DNA and cell-associated HIV RNA were quantified with a qPCR TaqMan assay using LTR-specific primers F522–43 (5′ GCC TCA ATA AAG CTT GCC TTG A 3′; HXB2522–543) and R626–43 (5′ GGG CGC CAC TGC TAG AGA 3′; 626–643) coupled with a FAMBQ probe (5′ CCA GAG TCA CAC AAC AGA CGG GCA CA 3) (Kumar et al., 2007) using the QuantStudio 6 Flex Real-Time PCR System (Applied Biosystems). Cell-associated HIV DNA copy number was determined using a reaction volume of 20 μL with 10 μL of 2x TaqMan Universal Master Mix II, including UNG (Applied Biosystems, cat# 4440038), 4 pmol of each primer, 4 pmol of probe, and 5 μL of DNA. Cycling conditions were 50°C for 2 min, 95°C for 10 min, followed by 60 cycles of 95°C for 15 s and 59°C for 1 min. External quantitation standards were prepared from DNA isolated from ACH-2 cells in a background of HIV-1 negative human cellular DNA, calibrated to the Virology Quality Assurance (VQA, NIH Division of AIDS) cellular DNA quantitation standards. Cell counts were determined by qPCR using human genomic TERT (Applied Biosystems, cat# 4403316). Copy number was determined by extrapolation against a 7-point standard curve (1–10,000 copies) performed in triplicate. Cell-associated HIV RNA copy number was determined using a reaction volume of 20 μL with 10 μL of 2x TaqMan® RNA to Ct 1 Step kit (Applied Biosystems, cat# 4392656), 4 pmol of each primer, 4 pmol of probe, 0.5 μL reverse transcriptase, and 5 μL of RNA. Cycling conditions were 48°C for 20 min, 95°C for 10 min, then 60 cycles of 95°C for 15 s and 59°C for 1 min. External quantitation standards were prepared from RNA isolated from NL4–3 virus, calibrated to the Virology Quality Assurance (VQA, NIH Division of AIDS) HIV RNA quantitation standards. Cell counts were determined by qPCR using human RPLP0 (Applied Biosystems, cat# 4310879E). Copy number was determined by extrapolation against a 7-point standard curve (1–10,000 copies) performed in triplicate.

Phenotypic characterization of SLe^{X+} and CLA^{+} $CD4^{+}$ T cells—Cryopreserved PBMC were thawed, counted, examined for viability and rested overnight at 37°C and 5% CO_2 in complete medium (RPMI supplemented with 10% FBS, 2 mM L-glutamine, 100 U/ml penicillin, and 100 mg/ml streptomycin). Cells were counted and plated for staining in 96-well V-bottom plates at 2–3 million cells per well. Stains for SLe^{X} stain and CLA analyses were performed in parallel. Cells were then stained for viability exclusion for 10 minutes at room temperature. The extracellular antibody cocktail mix containing either SLe^{x} or CLA was diluted in 1:1 Brilliant Stain Buffer Plus (BD Biosciences, cat# 566385) and FACS buffer (PBS with 0.1% sodium azide and 1% BSA), added and incubated at room temperature in the dark for 20 minutes. Cells were then washed and permeabilized using the eBiosciences FoxP3 Transcription Factor buffer kit (Invitrogen, cat# 00-5523-00) following the manufacturer's instructions. Intracellular antibody cocktail was incubated for one hour in

the dark. Following intracellular stain, cells were washed and fixed with PBS with 1% paraformaldehyde, and stored at 4°C in the dark until acquisition. Data were collected on a BD FACSymphony A5 flow cytometer (BD Biosciences) and analyzed using FlowJo software (Tree Star). The following antibodies were used for staining: CD3-BUV805 (clone UCHT1, BD Biosciences, cat# 565515), CD4-BB700 (clone SK3, BD Biosciences, cat# 566392), CD8-BUV496 (clone RPA-T8, BD Biosciences, cat# 564804), CD25-BUV737 (clone 2A3, BD Biosciences, cat# 564385), CD38-BUV661 (clone HIT2, BD Biosciences, cat# 565069), CD45RA-BUV563 (clone HI100, BD Biosciences, cat# 565702), CD69-PE (clone FN50, BD Biosciences, cat# 555531), CD127-BV480 (clone HIL-7RM21, BD Biosciences, cat# 566101), CCR4-PE-CF594 (clone 1G1, BD Biosciences, cat# 565391), CCR5-BV650 (clone 3A9, BD Biosciences, cat# 564999), CCR6-BV421 (clone 11A9, BD Biosciences, cat# 562515), CXCR4-PE Cy5 (clone 12G5, BD Biosciences, cat# 555975), CXCR5-BB515 (clone RF8B2, BD Biosciences, cat# 564624), HLA DR-BV605 (clone G46–6, BD Biosciences, cat# 562845), Ki67-BUV395 (clone B56, BD Biosciences, cat# 564071), SLe^X (CD15s)-AF647 (clone CSLEX1, BD Biosciences, cat# 563526), CD14-BV510 (clone M5E2, Biolegend, cat# 301842), CD19-BV510 (clone HIB19, Biolegend, cat# 302242), CD27-BV570 (clone O323, Biolegend, cat# 302825), CD95-BV711 (clone DX2, Biolegend, cat# 305644), CLA-AF647 (clone HECA-452, Biolegend, cat# 321309), CCR7-APC-Cy7 (clone G043H7, Biolegend, cat# 353211), CXCR3-AF700 (clone G025H7, Biolegend, cat# 353731) and PD-1-BV785 (clone EH12.2H7, Biolegend, cat# 329930). The FoxP3-PE Cy7 (clone 236A/E7, cat# 25-4777-42) antibody was purchased from eBioscience. The Invitrogen Live/Dead Fixable Aqua Dead Cell Stain Kit (Invitrogen, cat# L34955) was used for viability exclusion.

in vitro infection of unstimulated primary $CD4^+$ T cells without CD44 Microbeads—Isolated $CD4^+$ T cells from three healthy donors were incubated in RPMI 1640 medium supplemented with 10% FBS, L-glutamine (2 mM), penicillin (50 U/ml), streptomycin (50 mg/ml), and 30 U/ml IL-2. Cells were then spinoculated with either IIIB or 89.6 (PBS was used as a control) at a concentration of 50 ng of p24 per 1×10^6 cells for 2 h at 1,200 × g at 37°C. After spinoculation, all cells were returned to culture in the presence of 30 U/ml IL-2. Four days later, cells were stained with intracellular viral Gag p24 viral protein (PE-anti-p24 antibody; clone KC57, Beckman Coulter cat# 6604665) and SLe^X (BD biosciences, cat# 563526), or CLA (Biolegend, cat#321309). A violet viability dye for flow cytometry (Invitrogen, cat# L34955) was included to determine the cell viability. All samples were run on an LSR II flow cytometer and FACSDiva software. Data were analyzed with FlowJo.

CLA depletion from primary $CD4^+$ T cells—Five million purified $CD4^+$ T cells were incubated with anti-human/mouse CLA antibody (clone HECA-452, BioLegend, cat#321309) at 25 μg/ml in 1X PBS supplemented with 0.5% BSA at 4°C for 10 min. Cells were washed twice and further incubated with 25 μl anti-rat kappa MicroBeads (Miltenyi Biotec, cat# 130-047-401) for 15 min at 4°C. Cells were washed once and loaded onto pre-equilibrated LS columns (Miltenyi Biotec, cat#130-042-401) according to manufacturer's instructions. After washing extensively, cells in the eluate fraction were pelleted and

resuspended in RPMI 1640 medium supplemented with 10% FBS, L-glutamine (2 mM), penicillin (50 U/ml), streptomycin (50 mg/ml), and 30 U/ml IL-2.

Infection of unstimulated primary CD4$^+$ T cells using CD44 MicroBeads—CLA-depleted CD4$^+$ T cells from healthy donors were rested overnight in RPMI 1640 medium supplemented with 10% FBS, L-gluta-mine (2 mM), penicillin (50 U/ml), streptomycin (50 mg/ml), and 30 U/ml IL-2. 2 mL of CEMx174-grown HIV-1 DH12 (9,765,625 TCID50/ml) and 89.6 (5,710,972 TCID50/ml) were mixed with 100 µl of HIV Infectivity Enhancement Reagent (Miltenyi Biotec, cat# 130-095-093) and incubated at 4°C for 30 min. 500 µl of the virus-MicroBead mixture were then added to approximately 300,000 unstimulated CD4$^+$ T cells for 16 h in a 48 well culture plate. After overnight incubation, cells were washed once with 5 times volume of culture medium and incubated for additional 48 h at 37°C. Aliquots of virus exposed cells were taken from culture, washed with 1X PBS supplemented with 0.5% BSA and 0.1% sodium azide (FLOW buffer). Next, cells were stained with surface markers AF647-labeled anti-human/mouse CLA (clone HECA-452, BioLegend, cat# 321309) and AF647-labeled anti-human SLe^X (CD15s)-AF647 (clone CSLEX1, BD Biosciences, cat# 563526) in FLOW buffer for 30 min at room temperature protected from light. Cells were washed twice with 1 mL FLOW buffer and fixed using the Cytofix fixation buffer (BD BioSciences, cat# 554714) at 4°C for 20 min. After cell fixation, cells were permeabilized using the Perm/Wash buffer (BD BioSciences, cat# 554723) according to manufacturer's instructions before incubation with anti-p24 antibody (clone KC57, Beckman Coulter cat# 6604665) for 30 min at room temperature. Cells were washed, resuspended in FLOW buffer and acquired on a BD LSR-II (18 color).

Western blotting of glycosyltransferases and HIV p24 using H9 cell lysates—HIV-infected and uninfected H9 cells were pelleted and resuspended in radioimmunoprecipitation assay (RIPA) buffer (25 mM Tris-HCl pH 7.6, 150 mM NaCl, 1% NP-40, 1% sodium deoxycholate, 0.1% SDS) supplemented with protease inhibitor cocktail (Thermo Scientific, cat# 87786). After centrifugation, the protein concentration in the cell lysates was determined using Bicinchoninic acid (BCA) assay (Thermo Scientific, cat# 23235). 1 µg of total protein lysates were resolved on a 4%–12% Bis-Tris gel at 200 V for 30 min. Resolved proteins were transferred to nitrocellulose membranes, blocked and probed with the following primary antibodies: human Fucosyltransferase 7/FUT7 antibody, (clone 795116, R&D Systems, cat# MAB64091), B4GALT5 antibody (Novus, cat# NBP2–14882), GAPDH antibody (clone 14C10, Cell Signaling Technology, cat# 2118), anti-p24 antibody (clone KC57, Beckman Coulter cat# 6604665), and FUT6 Antibody (Thermo Fisher, cat# PA5–96261). After two washes in 1X TBS supplemented with 0.05% Tween 20, membranes were incubated with HRP-conjugated secondary antibody: Peroxidase AffiniPure Donkey Anti-Rabbit IgG (H+L) antibody (Jackson ImmunoResearch, cat# 711-035-152). Bound HRP-conjugated antibodies were revealed with SuperSignal West Pico PLUS chemiluminescent substrate (Thermo Scientific, cat# 34580).

in vitro stimulation of primary CD4$^+$ T cells—Isolated CD4$^+$ T cells from three healthy donors were incubated in RPMI 1640 medium supplemented with 10% FBS, L-glutamine (2 mM), penicillin (50 U/ml), and streptomycin (50 mg/ml). Cells were then

treated with αCD3/αCD28 activating beads (at a concentration of 1 bead/cell, GIBCO cat#11131D), TNF-α (10 ng/mL, Peprotech, cat# 300–01A), IL-2 (30 IU/ml, Peprotech, cat#200–20), IL-2+αCD3/αCD28, IL-2+TNF-α, or PBS as a control. Four days later, cells were stained with SLe^X (BD biosciences, cat#563526), or CLA (Biolegend, cat#321309). A violet viability dye for flow cytometry (Invitrogen, cat# L34955) was included to determine the cell viability. All samples were run on an LSR II flow cytometer and FACSDiva software. Data were analyzed with FlowJo.

CyTOF analysis of $CD4^+$ T cells isolated from HIV-infected ART-suppressed individuals—$CD4^+$ T cells were freshly isolated from the PBMCs of nine HIV-infected ART-suppressed individuals using the Human EasySep Human $CD4^+$ T Cell Isolation Kit (StemCell Technologies, cat#17952). Cells were fixed and stained with 25 μM cisplatin (cis-Diammine-platinum(II) dichloride, crystalline) (Sigma-Aldrich, cat# P4394–25MG) as a viability, washed, and then fixed with 2% PFA. To stain multiple samples at the same time, barcoding of cells was conducted using the Cell-ID 20-Plex Pd Barcoding Kit according to manufacturer's instructions (Fluidigm, cat# 201060). Barcoded samples were combined and blocked for 15 min on ice using sera from mouse (Thermo Fisher, cat# 501121171), rat (Thermo Fisher, cat# 10710C), and human (AB serum, Sigma-Aldrich, cat# H4522–20ML). Cells were then washed 2x with CyFACS buffer (metal contaminant-free PBS (Rockland, cat# MB-008) supplemented with 0.1% bovine serum albumin and 0.1% sodium azide) and stained with a cocktail of metal isotope-conjugated antibodies (Table S5). Antibody staining was performed in a total volume of 100 μL for 45 min on ice and followed by 3 washes with CyFACS buffer. After 3 washes with CyFACS buffer, cells were fixed overnight at 4°C with 2% PFA (Electron Microscopy Sciences) in metal contaminant-free PBS (Rockland). The next day, cells were permeabilized by incubation for 30 min at 4°C with fix/perm buffer (eBioscience, cat# 00-5523-00), and washed 2x with Permeabilization Buffer (eBioscience, cat# 00-5523-00). Cells were then blocked for 15 min on ice with sera from mouse (Thermo Fisher, cat# 501121171) and rat (Thermo Fisher, cat#10710C). After 2x washes with Permeabilization Buffer (eBioscience, cat# 00-5523-00), cells were stained for 45 min on ice with the Survivin antibody (R&D Systems, cat# MAB886) (Table S5). After another round of washing with CyFACS, cells were incubated for 20 min at room temperature with 250 nM Cell-ID™ DNA Intercalator-Ir (Fluidigm, cat# 201192A) in 2% PFA diluted in PBS. Prior to acquisition, cells were washed 2x with CyFACS, 1x with Maxpar® Cell Staining Buffer (Fluidigm, cat# 201068), 1x with Maxpar® PBS (Fluidigm, cat#201058), and 1x with Maxpar® Cell Acquisition Solution (Fluidigm, cat# 201240). Cells were then resuspended to a concentration of 7×10^5 / ml in EQ™ calibration beads (Fluidigm, cat# 201078) diluted in Maxpar® Cell Acquisition Solution. Cells were acquired at a rate of 250–350 events / sec on a CyTOF2 instrument (Fluidigm) at the UCSF Flow Cytometry Core. Data were normalized with EQ™ calibration beads and analyzed with FlowJo

RNA Sequencing—The NEBNext Ultra RNA Library Prep Kit for Illumina (New England Biolabs, cat# E7530S) was used to prepare the RNA sequencing libraries following the manufacturer's recommendations. Briefly, mRNA was enriched with Oligo d(T) beads. Enriched mRNAs were fragmented, and the first-strand and second-strand cDNA were then synthesized. cDNA fragments were end repaired and adenylated at 3′ ends, and a universal

adaptor was ligated to cDNA fragments, followed by index addition and library enrichment with limited cycle PCR. Sequencing libraries were validated using a DNA Chip on the Agilent 2100 Bioanalyzer (Agilent Technologies) and quantified by using Qubit 2.0 Fluorometer (Invitrogen) and quantitative PCR (Applied Biosystems). The sequencing libraries were multiplexed and clustered onto a flowcell. After clustering, the flowcell was loaded on the Illumina HiSeq 2500 instrument according to manufacturer's instructions. The samples were sequenced using a 2×50bp Paired Read (PR) configuration. Image analysis and base calling were conducted by the HiSeq Control Software (HCS) on the HiSeq 2500 instrument. Raw sequence data (.bcl files) generated from the Illumina HiSeq 2500 were converted into fastq files and de-multiplexed using the Illumina bcl2fastq v 1.8.4 program. The sequencing reactions were conducted at GENEWIZ, LLC.

RNASeq Analysis—RNA-seq data were aligned using *bowtie2* against the hg38 version of the human genome, and *RSEM* v1.2.12 software was used to estimate raw read counts and RPKM using Ensemble transcriptome information and *DESeq2* was used for raw count normalization and pairwise comparison between groups (Langmead and Salzberg, 2012; Li and Dewey, 2011; Love et al., 2014). Genes that changed at least 2 fold with FDR < 5% were considered significant. Gene set enrichment analysis was done using QIAGEN's Ingenuity® Pathway Analysis software (IPA®, QIAGEN Redwood City, https://digitalinsights.qiagen.com/) the Benjamini-Hochberg procedure to estimate the false discovery rate (FDR) (Benjamini et al., 2001). Select functions that passed $p < 10^{-7}$ and pathways that passed $p < 0.05$ significance threshold and had at least ten significant genes were reported. Predicted activation Z-score calculated by IPA based on the known effect and direction of change of membership genes.

QUANTIFICATION AND STATISTICAL ANALYSIS

Data were analyzed using Prism 6.0 and 7.0 (GraphPad Software). Mann-Whitney U-tests, Wilcoxson rank tests, paired t tests, Spearman's rank correlation coefficient tests, and Friedman tests were used. Statistical comparisons in Figures 1A–1D (n = 7) were performed using two-tailed non-parametric Wilcoxon rank tests. Statistical comparisons in Figures 1E and 1F (n = 6 for HIV-negative controls; 7 for HIV-infected ART-suppressed individuals, and 8 for HIV-infected viremic individuals) were performed using Mann-Whitney U-tests. All infection experiments in Figure 2 were conducted 3 times to ensure reproducibility and Paired t tests were used for statistical analysis. Friedman test (paired, non-parametric) was used for analysis in Figures 3 and 4 (n = 6 for HIV-negative controls; 7 for HIV-infected ART-suppressed individuals, and 8 for HIV-infected viremic individuals). Wilcoxon signed-rank test was used for statistical analysis in Figure 5 (n = 9). Statistical comparisons in Figure 6 (n = 4) were performed using paired t tests. False discovery rate (FDR) was calculated using the Benjamin-Hochberg procedure. For Figures 1, 2, 3, 4, and 5, Differences were considered statistically significant when the p value was less than 0.05, with * $p < 0.05$, ** $p < 0.01$, *** $p < 0.001$, **** $p < 0.0001$. FDR < 5% and 2 at least fold was considered significant in Figure 6. PCA and hierarchical clustering were performed using R-Studio.

Supplementary Material

Refer to Web version on PubMed Central for supplementary material.

ACKNOWLEDGMENTS

M.A.-M. is supported by NIH grants (R01 DK123733, R01 AG062383, R01 NS117458, R21 AI143385, R21 AI129636, and R21 NS106970), the Penn Center for AIDS Research (P30 AI 045008), and a Foundation for AIDS Research (amfAR) impact grant (109840-65-RGRL). Additional support was provided by the NIH-funded BEAT-HIV Martin Delaney Collaboratory to cure HIV-1 infection (1UM1Al126620), Kean Family Professorship, and Philadelphia Foundation (Roberts I. Jacobs Fund). N.R.R. is supported by NIH grants (R01 AI147777, R01 AI127219, and P01 AI131374). We thank all donor participants. We also thank Rachel E. Locke, Ph.D., for providing comments, and Mario Ostrowski, Ph.D., for providing PBMC from HIV-infected donors.

REFERENCES

Agrawal P, Fontanals-Cirera B, Sokolova E, Jacob S, Vaiana CA, Argibay D, Davalos V, McDermott M, Nayak S, Darvishian F, et al. (2017). A Systems Biology Approach Identifies FUT8 as a Driver of Melanoma Metastasis. Cancer Cell 31, 804–819. [PubMed: 28609658]

Barrera C, Espejo R, and Reyes VE (2002). Differential glycosylation of MHC class II molecules on gastric epithelial cells: implications in local immune responses. Hum. Immunol 63, 384–393. [PubMed: 11975982]

Battivelli E, Dahabieh MS, Abdel-Mohsen M, Svensson JP, Tojal Da Silva I, Cohn LB, Gramatica A, Deeks S, Greene WC, Pillai SK, and Verdin E (2018). Distinct chromatin functional states correlate with HIV latency reactivation in infected primary $CD4^+$ T cells. eLife 7, e34655. [PubMed: 29714165]

Benjamini Y, Drai D, Elmer G, Kafkafi N, and Golani I (2001). Controlling the false discovery rate in behavior genetics research. Behav. Brain Res 125, 279–284. [PubMed: 11682119]

Blanas A, Sahasrabudhe NM, Rodríguez E, van Kooyk Y, and van Vliet SJ (2018). Fucosylated Antigens in Cancer: An Alliance toward Tumor Progression, Metastasis, and Resistance to Chemotherapy. Front. Oncol 8, 39. [PubMed: 29527514]

Bosque A, and Planelles V (2009). Induction of HIV-1 latency and reactivation in primary memory CD4+ T cells. Blood 113, 58–65. [PubMed: 18849485]

Bruner KM, Murray AJ, Pollack RA, Soliman MG, Laskey SB, Capoferri AA, Lai J, Strain MC, Lada SM, Hoh R, et al. (2016). Defective proviruses rapidly accumulate during acute HIV-1 infection. Nat. Med 22, 1043–1049. [PubMed: 27500724]

Calvanese V, Chavez L, Laurent T, Ding S, and Verdin E (2013). Dual-color HIV reporters trace a population of latently infected cells and enable their purification. Virology 446, 283–292. [PubMed: 24074592]

Chan JK, and Greene WC (2011). NF-κB/Rel: agonist and antagonist roles in HIV-1 latency. Curr. Opin. HIV AIDS 6, 12–18. [PubMed: 21242888]

Chavez L, Calvanese V, and Verdin E (2015). HIV Latency Is Established Directly and Early in Both Resting and Activated Primary CD4 T Cells. PLoS Pathog 11, e1004955. [PubMed: 26067822]

Chomont N, El-Far M, Ancuta P, Trautmann L, Procopio FA, Yassine-Diab B, Boucher G, Boulassel MR, Ghattas G, Brenchley JM, et al. (2009). HIV reservoir size and persistence are driven by T cell survival and homeostatic proliferation. Nat. Med 15, 893–900. [PubMed: 19543283]

Chun TW, Carruth L, Finzi D, Shen X, DiGiuseppe JA, Taylor H, Hermankova M, Chadwick K, Margolick J, Quinn TC, et al. (1997). Quantification of latent tissue reservoirs and total body viral load in HIV-1 infection. Nature 387, 183–188. [PubMed: 9144289]

Colomb F, Giron LB, Premeaux TA, Mitchell BI, Niki T, Papasavvas E, Montaner LJ, Ndhlovu LC, and Abdel-Mohsen M (2019a). Galectin-9 Mediates HIV Transcription by Inducing TCR-Dependent ERK Signaling. Front. Immunol 10, 267. [PubMed: 30842775]

Colomb F, Giron LB, Trbojevic-Akmacic I, Lauc G, and Abdel-Mohsen M (2019b). Breaking the Glyco-Code of HIV Persistence and Immunopathogenesis. Curr. HIV/AIDS Rep 16, 151–168. [PubMed: 30707400]

de Freitas Junior JC, Silva Bdu.R., de Souza WF, de Araújo WM, Abdelhay ES, and Morgado-Díaz JA (2011). Inhibition of N-linked glycosylation by tunicamycin induces E-cadherin-mediated cell-cell adhesion and inhibits cell proliferation in undifferentiated human colon cancer cells. Cancer Chemother. Pharmacol 68, 227–238. [PubMed: 20927523]

Deeks SG (2011). HIV infection, inflammation, immunosenescence, and aging. Annu. Rev. Med 62, 141–155. [PubMed: 21090961]

Estes JD, Kityo C, Ssali F, Swainson L, Makamdop KN, Del Prete GQ, Deeks SG, Luciw PA, Chipman JG, Beilman GJ, et al. (2017). Defining total-body AIDS-virus burden with implications for curative strategies. Nat. Med 23, 1271–1276. [PubMed: 28967921]

Everest-Dass AV, Jin D, Thaysen-Andersen M, Nevalainen H, Kolarich D, and Packer NH (2012). Comparative structural analysis of the glycosylation of salivary and buccal cell proteins: innate protection against infection by Candida albicans. Glycobiology 22, 1465–1479. [PubMed: 22833316]

Finzi D, Hermankova M, Pierson T, Carruth LM, Buck C, Chaisson RE, Quinn TC, Chadwick K, Margolick J, Brookmeyer R, et al. (1997). Identification of a reservoir for HIV-1 in patients on highly active antiretroviral therapy. Science 278, 1295–1300. [PubMed: 9360927]

Friedrich M, Bock D, Philipp S, Ludwig N, Sabat R, Wolk K, Schroeter-Maas S, Aydt E, Kang S, Dam TN, et al. (2006). Pan-selectin antagonism improves psoriasis manifestation in mice and man. Arch. Dermatol. Res 297, 345–351. [PubMed: 16362415]

Fromentin R, Bakeman W, Lawani MB, Khoury G, Hartogensis W, Da-Fonseca S, Killian M, Epling L, Hoh R, Sinclair E, et al. (2016). CD4+ T Cells Expressing PD-1, TIGIT and LAG-3 Contribute to HIV Persistence during ART. PLoS Pathog 12, e1005761. [PubMed: 27415008]

Giron LB, Papasavvas E, Azzoni L, Yin X, Anzurez A, Damra M, Mounzer K, Kostman JR, Sanne I, Firnhaber CS, et al. (2020a). Plasma and antibody glycomic biomarkers of time to HIV rebound and viral setpoint. AIDS 34, 681–686. [PubMed: 31972605]

Giron LB, Tanes CE, Schleimann MH, Engen PA, Mattei LM, Anzurez A, Damra M, Zhang H, Bittinger K, Bushman F, et al. (2020b). Sialylation and fucosylation modulate inflammasome-activating eIF2 Signaling and microbial translocation during HIV infection. Mucosal Immunol Published online March 9, 2020. 10.1038/s41385-020-0279-5.

Gosselin A, Wiche Salinas TR, Planas D, Wacleche VS, Zhang Y, Fromentin R, Chomont N, Cohen EA, Shacklett B, Mehraj V, et al. (2017). HIV persists in CCR6+CD4+ T cells from colon and blood during antiretroviral therapy. AIDS 31, 35–48. [PubMed: 27835617]

Haddad W, Cooper CJ, Zhang Z, Brown JB, Zhu Y, Issekutz A, Fuss I, Lee HO, Kansas GS, and Barrett TA (2003). P-selectin and P-selectin glycoprotein ligand 1 are major determinants for Th1 cell recruitment to non-lymphoid effector sites in the intestinal lamina propria. J. Exp. Med 198, 369–377. [PubMed: 12885868]

Hirabayashi J, Yamada M, Kuno A, and Tateno H (2013). Lectin microarrays: concept, principle and applications. Chem. Soc. Rev 42, 4443–4458. [PubMed: 23443201]

Hirabayashi J, Kuno A, and Tateno H (2015). Development and Applications of the Lectin Microarray. Top. Curr. Chem 367, 105–124. [PubMed: 25821171]

Hiraiwa N, Hiraiwa M, and Kannagi R (1997). Human T-cell leukemia virus-1 encoded Tax protein transactivates alpha 1/3 fucosyltransferase Fuc-T VII, which synthesizes sialyl Lewis X, a selectin ligand expressed on adult T-cell leukemia cells. Biochem. Biophys. Res. Commun 231, 183–186. [PubMed: 9070245]

Hiraiwa N, Yabuta T, Yoritomi K, Hiraiwa M, Tanaka Y, Suzuki T, Yoshida M, and Kannagi R (2003). Transactivation of the fucosyltransferase VII gene by human T-cell leukemia virus type 1 Tax through a variant cAMP-responsive element. Blood 101, 3615–3621. [PubMed: 12506041]

Ho YC, Shan L, Hosmane NN, Wang J, Laskey SB, Rosenbloom DI, Lai J, Blankson JN, Siliciano JD, and Siliciano RF (2013). Replication-competent noninduced proviruses in the latent reservoir increase barrier to HIV-1 cure. Cell 155, 540–551. [PubMed: 24243014]

Hogan LE, Vasquez J, Hobbs KS, Hanhauser E, Aguilar-Rodriguez B, Hussien R, Thanh C, Gibson EA, Carvidi AB, Smith LCB, et al. (2018). Increased HIV-1 transcriptional activity and infectious burden in peripheral blood and gut-associated CD4+ T cells expressing CD30. PLoS Pathog 14, e1006856. [PubMed: 29470552]

Huang YL, Hung JT, Cheung SK, Lee HY, Chu KC, Li ST, Lin YC, Ren CT, Cheng TJ, Hsu TL, et al. (2013). Carbohydrate-based vaccines with a glycolipid adjuvant for breast cancer. Proc. Natl. Acad. Sci. USA 110, 2517–2522. [PubMed: 23355685]

Iglesias-Ussel M, Vandergeeten C, Marchionni L, Chomont N, and Romerio F (2013). High levels of CD2 expression identify HIV-1 latently infected resting memory CD4+ T cells in virally suppressed subjects. J. Virol 87, 9148–9158. [PubMed: 23760244]

Imamichi H, Smith M, Adelsberger JW, Izumi T, Scrimieri F, Sherman BT, Rehm CA, Imamichi T, Pau A, Catalfamo M, et al. (2020). Defective HIV-1 proviruses produce viral proteins. Proc. Natl. Acad. Sci. USA 117, 3704–3710. [PubMed: 32029589]

Impellizzeri D, and Cuzzocrea S (2014). Targeting selectins for the treatment of inflammatory diseases. Expert Opin. Ther. Targets 18, 55–67. [PubMed: 24074033]

Julien S, Ivetic A, Grigoriadis A, QiZe D, Burford B, Sproviero D, Picco G, Gillett C, Papp SL, Schaffer L, et al. (2011). Selectin ligand sialyl-Lewis x antigen drives metastasis of hormone-dependent breast cancers. Cancer Res 71, 7683–7693. [PubMed: 22025563]

Kambara C, Nakamura T, Furuya T, Nishiura Y, Kawakami A, Ichinose K, Shirabe S, and Eguchi K (2002). Increased sialyl Lewis(x) antigen-positive cells mediated by HTLV-1 infection in peripheral blood CD4(+) T lymphocytes in patients with HTLV-1-associated myelopathy. J. Neuroimmunol 125, 179–184. [PubMed: 11960655]

Kim Y, Cameron PU, Lewin SR, and Anderson JL (2019). Limitations of dual-fluorescent HIV reporter viruses in a model of pre-activation latency. J. Int. AIDS Soc 22, e25425. [PubMed: 31855322]

Kirsten A, Watz H, Kretschmar G, Pedersen F, Bock D, Meyer-Sabellek W, and Magnussen H (2011). Efficacy of the pan-selectin antagonist Bimosiamose on ozone-induced airway inflammation in healthy subjects—a double blind, randomized, placebo-controlled, cross-over clinical trial. Pulm. Pharmacol. Ther 24, 555–558. [PubMed: 21514398]

Kumar AM, Borodowsky I, Fernandez B, Gonzalez L, and Kumar M (2007). Human immunodeficiency virus type 1 RNA Levels in different regions of human brain: quantification using real-time reverse transcriptase-polymerase chain reaction. J. Neurovirol 13, 210–224. [PubMed: 17613711]

Kuo H-H, Ahmad R, Lee GQ, Gao C, Chen H-R, Ouyang Z, Szucs MJ, Kim D, Tsibris A, Chun T-W, et al. (2018). Anti-apoptotic Protein BIRC5 Maintains Survival of HIV-1-Infected $CD4^+$ T Cells. Immunity 48, 1183–1194. [PubMed: 29802019]

Kuzmanov U, Jiang N, Smith CR, Soosaipillai A, and Diamandis EP (2009). Differential N-glycosylation of kallikrein 6 derived from ovarian cancer cells or the central nervous system. Mol. Cell. Proteomics 8, 791–798. [PubMed: 19088065]

Langmead B, and Salzberg SL (2012). Fast gapped-read alignment with Bowtie 2. Nat. Methods 9, 357–359. [PubMed: 22388286]

Ley K, Laudanna C, Cybulsky MI, and Nourshargh S (2007). Getting to the site of inflammation: the leukocyte adhesion cascade updated. Nat. Rev. Immunol 7, 678–689. [PubMed: 17717539]

Li B, and Dewey CN (2011). RSEM: accurate transcript quantification from RNA-Seq data with or without a reference genome. BMC Bioinformatics 12, 323. [PubMed: 21816040]

Liang W, Mao S, Sun S, Li M, Li Z, Yu R, Ma T, Gu J, Zhang J, Taniguchi N, and Li W (2018). Core Fucosylation of the T Cell Receptor Is Required for T Cell Activation. Front. Immunol 9, 78. [PubMed: 29434598]

Love MI, Huber W, and Anders S (2014). Moderated estimation of fold change and dispersion for RNA-seq data with DESeq2. Genome Biol 15, 550. [PubMed: 25516281]

Mayr FB, Firbas C, Leitner JM, Spiel AO, Reiter RA, Beyer D, Meyer M, Wolff G, and Jilma B (2008). Effects of the pan-selectin antagonist bimosiamose (TBC1269) in experimental human endotoxemia. Shock 29, 475–482. [PubMed: 18598003]

Mbonye U, and Karn J (2014). Transcriptional control of HIV latency: cellular signaling pathways, epigenetics, happenstance and the hope for a cure. Virology 454–455, 328–339.

McGary CS, Deleage C, Harper J, Micci L, Ribeiro SP, Paganini S, Kuri-Cervantes L, Benne C, Ryan ES, Balderas R, et al. (2017). CTLA-4^+PD-1^- Memory $CD4^+$ T Cells Critically Contribute to

Viral Persistence in Antiretroviral Therapy-Suppressed, SIV-Infected Rhesus Macaques. Immunity 47, 776–788. [PubMed: 29045906]

Misonou Y, Shida K, Korekane H, Seki Y, Noura S, Ohue M, and Miya-moto Y (2009). Comprehensive clinico-glycomic study of 16 colorectal cancer specimens: elucidation of aberrant glycosylation and its mechanistic causes in colorectal cancer cells. J. Proteome Res 8, 2990–3005. [PubMed: 19292502]

Nagahara K, Arikawa T, Oomizu S, Kontani K, Nobumoto A, Tateno H, Watanabe K, Niki T, Katoh S, Miyake M, et al. (2008). Galectin-9 increases Tim-3+ dendritic cells and CD8+ T cells and enhances antitumor immunity via galectin-9-Tim-3 interactions. J. Immunol 181, 7660–7669. [PubMed: 19017954]

Nakamori S, Kameyama M, Imaoka S, Furukawa H, Ishikawa O, Sasaki Y, Izumi Y, and Irimura T (1997). Involvement of carbohydrate antigen sialyl Lewis(x) in colorectal cancer metastasis. Dis. Colon Rectum 40, 420–431. [PubMed: 9106690]

Nyström K, Grahn A, Lindh M, Brytting M, Mandel U, Larson G, and Olofsson S (2007). Virus-induced transcriptional activation of host FUT genes associated with neo-expression of Ley in cytomegalovirus-infected and sialyl-Lex in varicella-zoster virus-infected diploid human cells. Glycobiology 17, 355–366. [PubMed: 17202152]

Nyström K, Nordén R, Muylaert I, Elias P, Larson G, and Olofsson S (2009). Induction of sialyl-Lex expression by herpes simplex virus type 1 is dependent on viral immediate early RNA-activated transcription of host fucosyltransferase genes. Glycobiology 19, 847–859. [PubMed: 19369700]

Okada M, Chikuma S, Kondo T, Hibino S, Machiyama H, Yokosuka T, Nakano M, and Yoshimura A (2017). Blockage of Core Fucosylation Reduces Cell-Surface Expression of PD-1 and Promotes Anti-tumor Immune Responses of T Cells. Cell Rep 20, 1017–1028. [PubMed: 28768188]

Pereira MS, Alves I, Vicente M, Campar A, Silva MC, Padrão NA, Pinto V, Fernandes Â, Dias AM, and Pinho SS (2018). Glycans as Key Checkpoints of T Cell Activity and Function. Front. Immunol 9, 2754. [PubMed: 30538706]

Pinho SS, and Reis CA (2015). Glycosylation in cancer: mechanisms and clinical implications. Nat. Rev. Cancer 15, 540–555. [PubMed: 26289314]

Pollack RA, Jones RB, Pertea M, Bruner KM, Martin AR, Thomas AS, Capoferri AA, Beg SA, Huang S-H, Karandish S, et al. (2017). Defective HIV-1 Proviruses Are Expressed and Can Be Recognized by Cytotoxic T Lymphocytes, which Shape the Proviral Landscape. Cell Host Microbe 21, 494–506. [PubMed: 28407485]

Rodríguez E, Schetters STT, and van Kooyk Y (2018). The tumour glycocode as a novel immune checkpoint for immunotherapy. Nat. Rev. Immunol 18, 204–211. [PubMed: 29398707]

Serra-Peinado C, Grau-Expósito J, Luque-Ballesteros L, Astorga-Gamaza A, Navarro J, Gallego-Rodriguez J, Martin M, Curran A, Burgos J, Ribera E, et al. (2019). Expression of CD20 after viral reactivation renders HIV-reservoir cells susceptible to Rituximab. Nat. Commun 10, 3705. [PubMed: 31420544]

Tateno H, Uchiyama N, Kuno A, Togayachi A, Sato T, Narimatsu H, and Hirabayashi J (2007). A novel strategy for mammalian cell surface glycome profiling using lectin microarray. Glycobiology 17, 1138–1146. [PubMed: 17693441]

Tateno H, Nakamura-Tsuruta S, and Hirabayashi J (2009). Comparative analysis of core-fucose-binding lectins from Lens culinaris and Pisum sativum using frontal affinity chromatography. Glycobiology 19, 527–536. [PubMed: 19218400]

Tateno H, Kuno A, Itakura Y, and Hirabayashi J (2010). A versatile technology for cellular glycomics using lectin microarray. Methods Enzymol 478, 181–195. [PubMed: 20816480]

Tateno H, Toyota M, Saito S, Onuma Y, Ito Y, Hiemori K, Fukumura M, Matsushima A, Nakanishi M, Ohnuma K, et al. (2011). Glycome diagnosis of human induced pluripotent stem cells using lectin microarray. J. Biol. Chem 286, 20345–20353. [PubMed: 21471226]

Telen MJ, Wun T, McCavit TL, De Castro LM, Krishnamurti L, Lanzkron S, Hsu LL, Smith WR, Rhee S, Magnani JL, and Thackray H (2015). Randomized phase 2 study of GMI-1070 in SCD: reduction in time to resolution of vaso-occlusive events and decreased opioid use. Blood 125, 2656–2664. [PubMed: 25733584]

Terry VH, Johnston IC, and Spina CA (2009). CD44 microbeads accelerate HIV-1 infection in T cells. Virology 388, 294–304. [PubMed: 19394995]

Trinchera M, Aronica A, and Dall'Olio F (2017). Selectin Ligands Sialyl-Lewis a and Sialyl-Lewis x in Gastrointestinal Cancers. Biology (Basel) 6, 16.

Uchiyama N, Kuno A, Tateno H, Kubo Y, Mizuno M, Noguchi M, and Hirabayashi J (2008). Optimization of evanescent-field fluorescence-assisted lectin microarray for high-sensitivity detection of monovalent oligosaccharides and glycoproteins. Proteomics 8, 3042–3050. [PubMed: 18615430]

Umehara F, Izumo S, Takeya M, Takahashi K, Sato E, and Osame M (1996). Expression of adhesion molecules and monocyte chemoattractant protein −1 (MCP-1) in the spinal cord lesions in HTLV-I-associated myelopathy. Acta Neuropathol 91, 343–350. [PubMed: 8928610]

Williams GJ, and Thorson JS (2009). Natural product glycosyltransferases: properties and applications. Adv. Enzymol. Relat. Areas Mol. Biol 76, 55–119. [PubMed: 18990828]

Wolber FM, Curtis JL, Mály P, Kelly RJ, Smith P, Yednock TA, Lowe JB, and Stoolman LM (1998). Endothelial selectins and alpha4 integrins regulate independent pathways of T lymphocyte recruitment in the pulmonary immune response. J. Immunol 161, 4396–4403. [PubMed: 9780218]

Wong JK, Hezareh M, Günthard HF, Havlir DV, Ignacio CC, Spina CA, and Richman DD (1997). Recovery of replication-competent HIV despite prolonged suppression of plasma viremia. Science 278, 1291–1295. [PubMed: 9360926]

Xie H, Lim YC, Luscinskas FW, and Lichtman AH (1999). Acquisition of selectin binding and peripheral homing properties by CD4(+) and CD8(+) T cells. J. Exp. Med 189, 1765–1776. [PubMed: 10359580]

Yukl SA, Kaiser P, Kim P, Telwatte S, Joshi SK, Vu M, Lampiris H, and Wong JK (2018). HIV latency in isolated patient $CD4^+$ T cells may be due to blocks in HIV transcriptional elongation, completion, and splicing. Sci. Transl. Med 10, eaap9927. [PubMed: 29491188]

Highlights

- Persistent HIV transcription modulates the glycosylation of infected cells
- Cells actively transcribing HIV harbor high levels of fucosylated carbohydrates
- HIV transcription induces the fucosylated extravasation mediator, Sialyl-Lewis^X
- Cells with high Sialyl-Lewis^X are enriched with pathways involved in trafficking

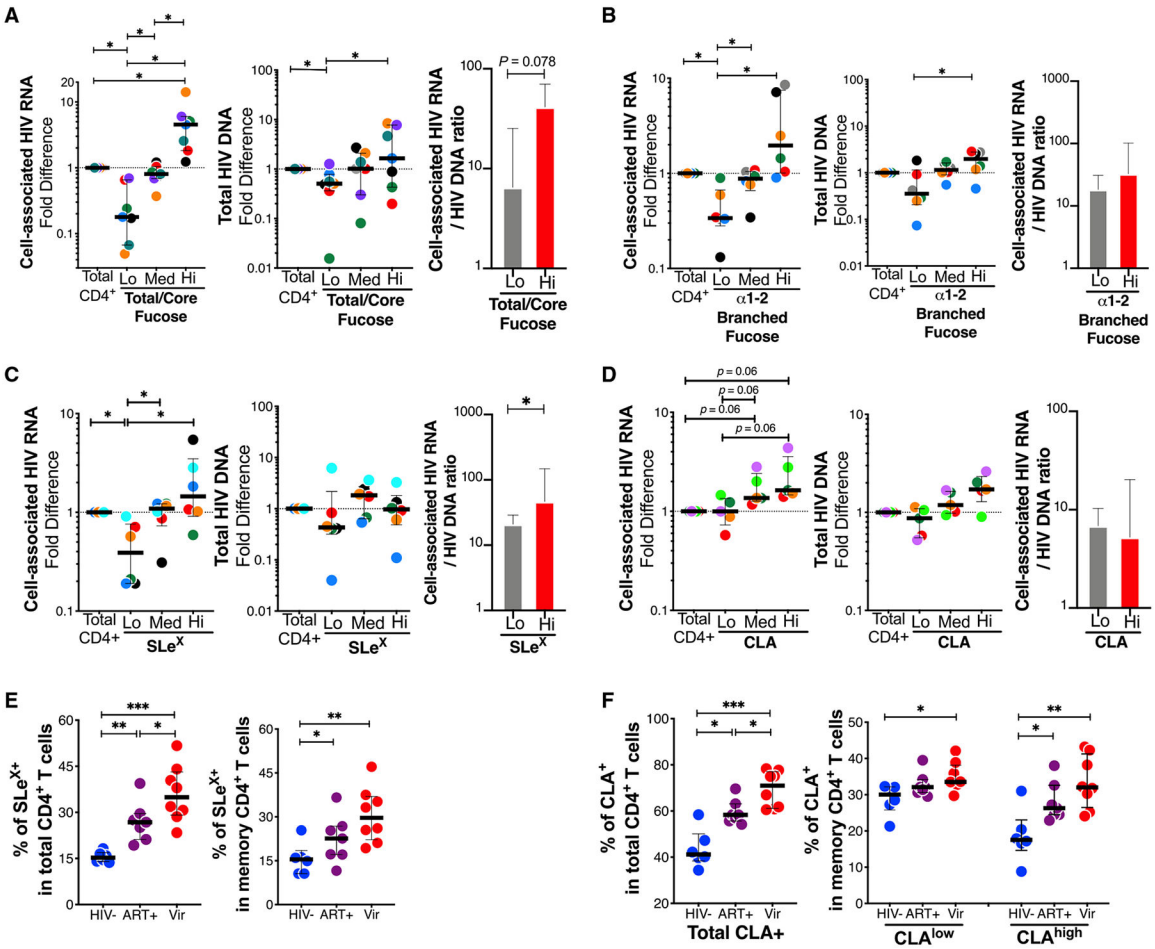

Figure 1. CD4$^+$ T Cell-Surface Fucosylation and SLe^X Expression Associate with Persistent HIV Transcription In Vivo

(A–D) CD4$^+$ T cells from HIV-infected ART-suppressed individuals were sorted based on levels of cell-surface fucosylation, SLe^X, or CLA expression (lowest 5%, medium, and highest 5%); levels of HIV DNA and cell-associated HIV RNA (total elongated transcripts) were measured by qPCR. The ratio of cell-associated HIV RNA to HIV DNA was calculated.

(A and B) Cells with high fucose, either total/core (A) or branched (B), exhibited higher levels of cell-associated HIV RNA compared with cells with low fucose, despite a less dramatic difference in levels of HIV DNA.

(C and D) Cells with high levels of SLe^X (C) or CLA (D) exhibited higher levels of cell-associated HIV RNA compared with cells with low levels of SLe^X or CLA, despite similar levels of HIV DNA *in vivo*. Furthermore, cells with SLe$^{X\text{-}Hi}$ exhibited higher ratio of cell-associated HIV RNA to HIV DNA compared with cells with SLe$^{X\text{-}Low}$ (C). Lines and error bars represent the median and IQR. All statistical comparisons were performed using two-tailed non-parametric Wilcoxon rank tests. *p < 0.05.

(E and F) Percentage of SLe^X (E) and CLA (F) within total and memory CD4$^+$ T cells of HIV-negative, HIV-infected ART-suppressed, and HIV-infected viremic individuals.

Lines and error bars represent the median and IQR. Statistical comparisons were performed using two-tailed non-parametric Mann-Whitney U tests. n = 6 for HIV-negative controls; 7 for HIV-infected ART-suppressed individuals, and 8 for HIV-infected viremic individuals. *$p < 0.05$, **$p < 0.01$, ***$p < 0.001$.

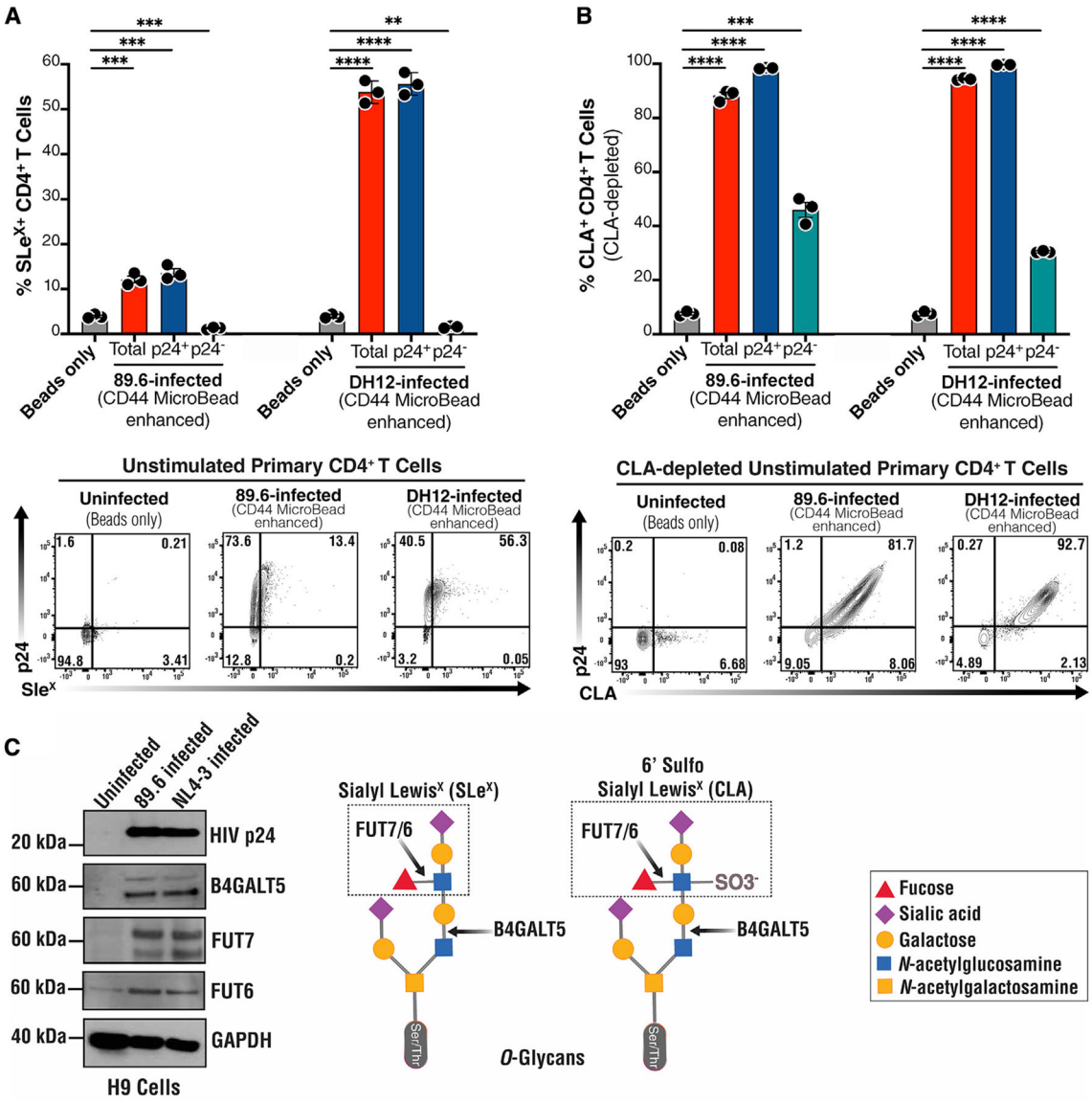

Figure 2. HIV Infection Induces the Expression of SLe^X and CLA on the Surface of Primary CD4$^+$ T Cells In Vitro

(A) Isolated CD4$^+$ T cells from three HIV-negative donors were infected with either the HIV 89.6 virus (at a multiplicity of infection [MOI] of 6) or the HIV DH12 virus (at MOI of 10) by spinoculation in the presence of CD44 MicroBeads. Four days later, intracellular p24 expression and cell-surface expression of SLe^X were determined by flow cytometry.

(B) Isolated CD4$^+$ T cells from three HIV-negative donors were depleted of CLA$^+$ cells. CLA-depleted cells were infected with either HIV 89.6 or HIV DH12 by spinoculation in the presence of CD44 MicroBeads. Four days later, intracellular p24 expression and cell-surface expression of CLA were determined by flow cytometry. (A and B) Top panels show the percentage of SLe^X or CLA on total, p24+, and p24-negative cells, as well as controls (cells treated with CD44 MicroBeads alone), for each HIV strain. Bottom panels are representative flow cytometry plots of dually stained CD4$^+$ T cells for HIV p24 protein and

SLe^X or CLA. Mean and standard error of the mean (SEM) are presented. Paired t tests were used for statistical analysis.

(C) H9 cell line was infected with either HIV 89.6 (MOI of 6) or NL4–3 (MOI of 0.1) in the presence of CD44 MicroBeads. Protein expression of several glycosyltransferases involved in SLe^X and CLA production (FUT6, FUT7, and B4GALT5), as well as HIV p24, was measured by western blotting. Diagrams show locations of glycosidic bonds catalyzed by indicated glycosyltransferases.

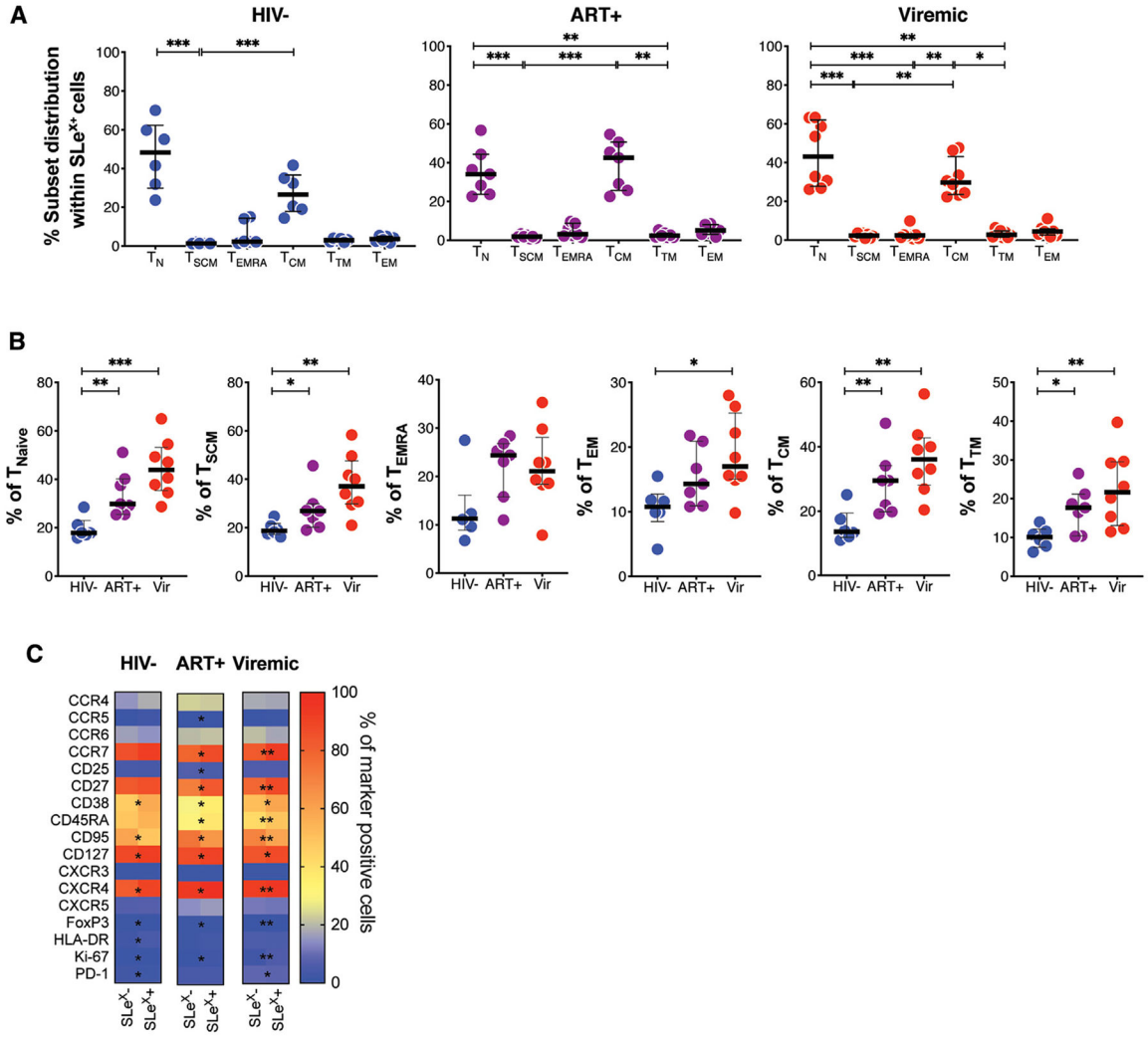

Figure 3. SLe^X Expression Is Enriched on T_{CM} and Naive $CD4^+$ and Associates with Higher Activation Status

(A) Memory subset distribution of SLe^{X+} cells in HIV^-, HIV^+ ART-suppressed, and HIV^+ viremic donors.

(B) Frequency of SLe^{X+} cells within each memory $CD4^+$ T cell subset in the analyzed groups. Subsets were defined as T_N (naive; $CD45RA^+$ $CD27^+$ $CCR7^+$ $CD95^-$), T_{SCM} (stem cell memory; $CD45RA^+$ $CD27^+$ $CCR7^+$ $CD95^+$), T_{EMRA} (effector memory RA^+; $CD45RA^+$ $CD27^-$), T_{EM} (effector memory; $CD45RA^-$ $CD27^-CCR7^-$), T_{CM} (central memory; $CD45RA^-$ $CD27^+$ $CCR7^+$), and T_{TM} (transitional memory; $CD45RA^-$ $CD27^+$ $CCR7^-$). Lines and error bars represent the median and IQR. All statistical comparisons were performed using two-tailed Wilcoxon rank tests.

(C) Heatmaps showing the statistical difference in the frequency of all measured phenotypic markers in SLe^{X+} and SLe^{X-} cells.

All data were analyzed using a Friedman test (paired, non-parametric). n = 6 for HIV^-, 7 for HIV^+ ART-suppressed individuals, and 8 for HIV^+ viremic individuals. *p < 0.05, **p < 0.01, ***p < 0.001.

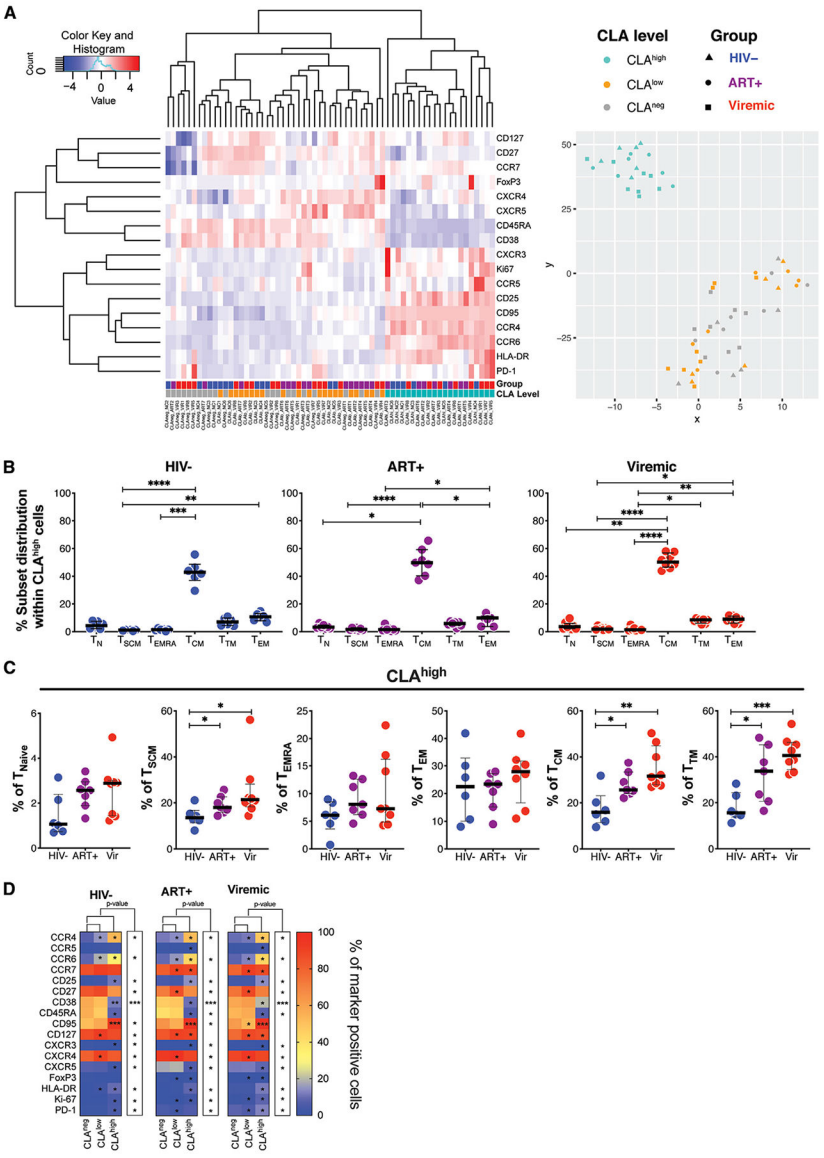

Figure 4. CLA^{high} CD4^{+} T Cells Cluster Distinctly from CLA^{low} and CLA^{negative} CD4^{+} T Cells

(A) Left, heatmap showing the frequency of all measured phenotypic markers in CLA^{high}, CLA^{low}, and CLA^{-} cells. Right, PCA showing the distribution of CLA^{high}, CLA^{low}, and CLA^{-} cells subsets.

(B) Memory subset distribution of CLA^{high} cells in HIV^{-}, HIV^{+} ART-treated, and HIV^{+} viremic individuals.

(C) Frequency of CLA^{high} cells within each memory CD4^{+} T cell subset in the analyzed groups. Lines and error bars represent the median and IQR. All statistical comparisons were performed using two-tailed Wilcoxon rank tests.

(D) Heatmaps showing the statistical difference in the frequency of all measured phenotypic markers CLA^{high}, CLA^{low}, and CLA^{-} cells.

All data were analyzed using a Friedman test (paired, non-parametric). n = 6 for HIV^-, 7 for HIV^+ ART-suppressed individuals, and 8 for HIV^+ viremic individuals. *$p < 0.05$, **$p < 0.01$, ***$p < 0.001$.

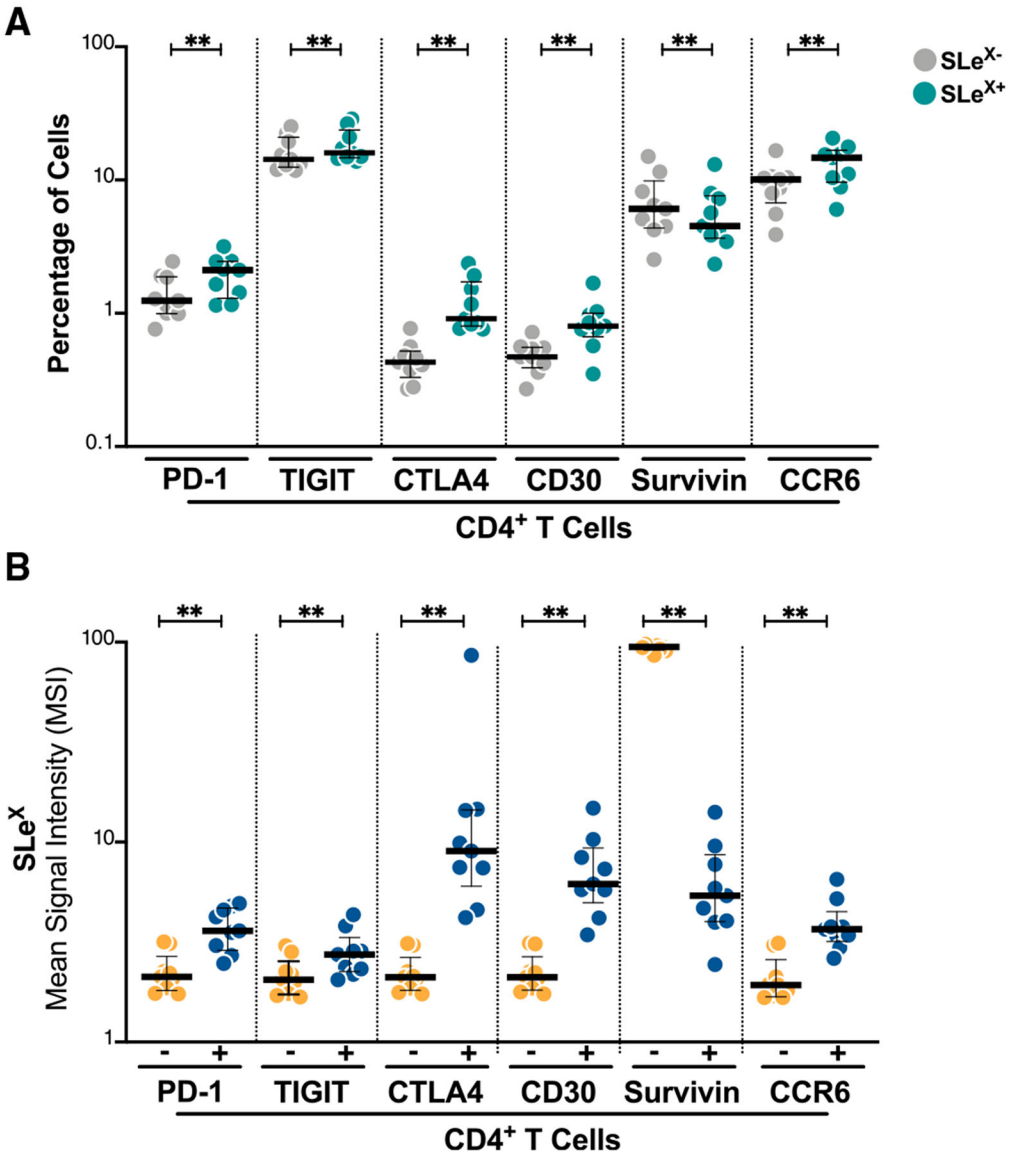

Figure 5. SLe^{X+} and SLe^{X-} $CD4^+$ T Cells Have Differential Levels of Host Factors Known to Be Enriched in HIV-Infected Cells during ART

CyTOF analysis of $CD4^+$ T cells freshly isolated from PBMCs of nine HIV-infected ART-suppressed individuals. Cells were stained for SLe^X, PD-1, TIGIT, CTLA-4, CD30, CCR6, or Survivin.

(A) Percentage of SLe^{X+} and SLe^{X-} $CD4^+$ T cells expressing each of the indicated factors.

(B) Mean signal intensity of SLe^X on the surface of cells expressing or not each of the indicated factors.

Median and IQR are presented, and p values were calculated using Wilcoxon signed-rank test. **$p < 0.01$.

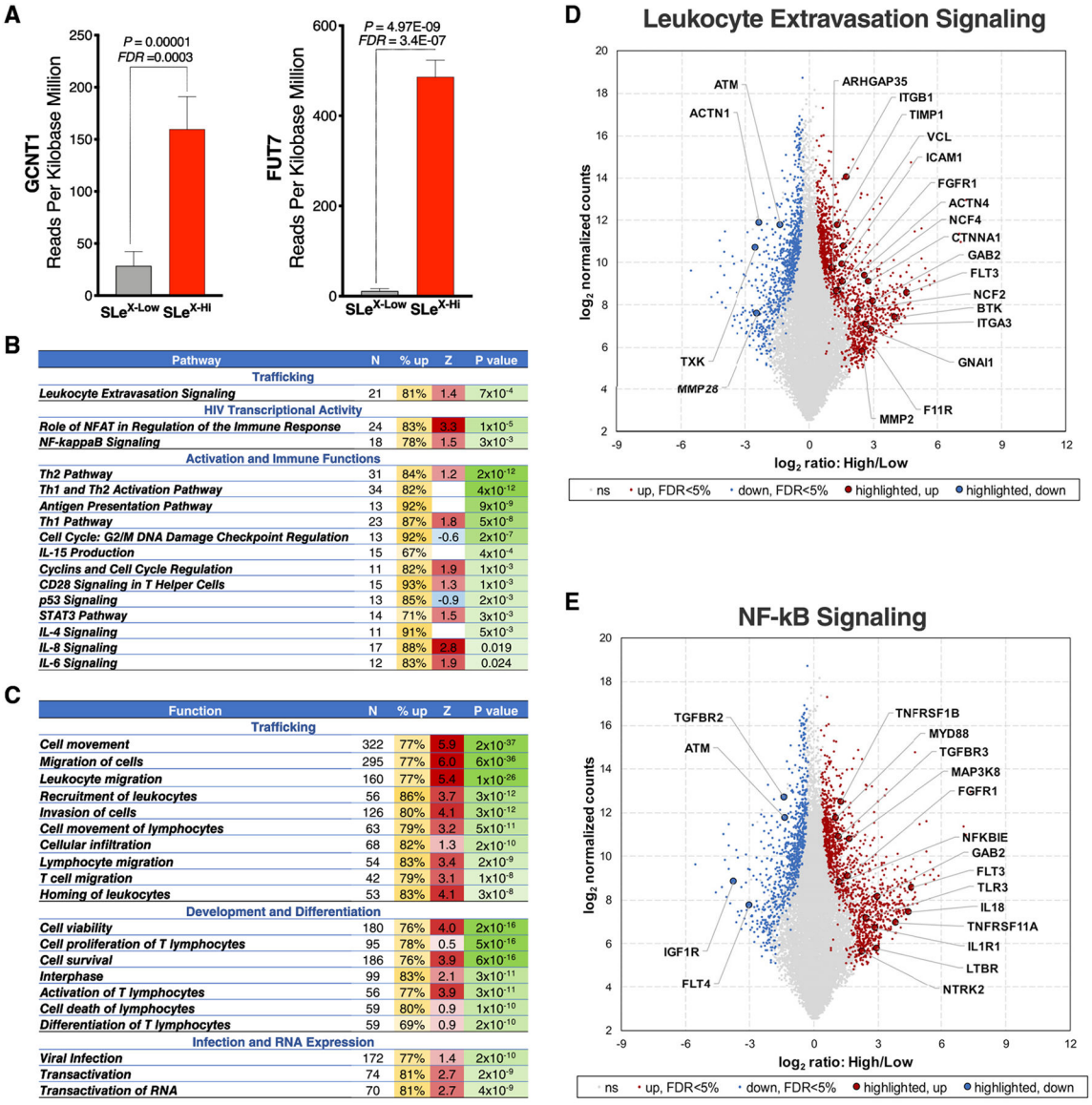

B

Pathway	N	% up	Z	P value
Trafficking				
Leukocyte Extravasation Signaling	21	81%	1.4	$7x10^{-4}$
HIV Transcriptional Activity				
Role of NFAT in Regulation of the Immune Response	24	83%	3.3	$1x10^{-5}$
NF-kappaB Signaling	18	78%	1.5	$3x10^{-3}$
Activation and Immune Functions				
Th2 Pathway	31	84%	1.2	$2x10^{-12}$
Th1 and Th2 Activation Pathway	34	82%		$4x10^{-12}$
Antigen Presentation Pathway	13	92%		$9x10^{-9}$
Th1 Pathway	23	87%	1.8	$5x10^{-8}$
Cell Cycle: G2/M DNA Damage Checkpoint Regulation	13	92%	-0.6	$2x10^{-7}$
IL-15 Production	15	67%		$4x10^{-4}$
Cyclins and Cell Cycle Regulation	11	82%	1.9	$1x10^{-3}$
CD28 Signaling in T Helper Cells	15	93%	1.3	$1x10^{-3}$
p53 Signaling	13	85%	-0.9	$2x10^{-3}$
STAT3 Pathway	14	71%	1.5	$3x10^{-3}$
IL-4 Signaling	11	91%		$5x10^{-3}$
IL-8 Signaling	17	88%	2.8	0.019
IL-6 Signaling	12	83%	1.9	0.024

C

Function	N	% up	Z	P value
Trafficking				
Cell movement	322	77%	5.9	$2x10^{-37}$
Migration of cells	295	77%	6.0	$6x10^{-36}$
Leukocyte migration	160	77%	5.4	$1x10^{-26}$
Recruitment of leukocytes	56	86%	3.7	$3x10^{-12}$
Invasion of cells	126	80%	4.1	$3x10^{-12}$
Cell movement of lymphocytes	63	79%	3.2	$5x10^{-11}$
Cellular infiltration	68	82%	1.3	$2x10^{-10}$
Lymphocyte migration	54	83%	3.4	$2x10^{-9}$
T cell migration	42	79%	3.1	$1x10^{-8}$
Homing of leukocytes	53	83%	4.1	$3x10^{-8}$
Development and Differentiation				
Cell viability	180	76%	4.0	$2x10^{-16}$
Cell proliferation of T lymphocytes	95	78%	0.5	$5x10^{-16}$
Cell survival	186	76%	3.9	$6x10^{-16}$
Interphase	99	83%	2.1	$3x10^{-11}$
Activation of T lymphocytes	56	77%	3.9	$3x10^{-11}$
Cell death of lymphocytes	59	80%	0.9	$1x10^{-10}$
Differentiation of T lymphocytes	59	69%	0.9	$2x10^{-10}$
Infection and RNA Expression				
Viral Infection	172	77%	1.4	$2x10^{-10}$
Transactivation	74	81%	2.7	$2x10^{-9}$
Transactivation of RNA	70	81%	2.7	$4x10^{-9}$

Figure 6. SLe^{X+} CD4^{+} T Cells Are Enriched for Pathways Involved in T Cell Extravasation and HIV Transcription

(A) Relative expression of GCNT1 and FUT7 genes in SLe^{X-Hi} and SLe^{X-Low} CD4^{+} T cells isolated from four HIV^{+} ART-suppressed individuals. Mean and SEM are presented, and p values were calculated using paired t tests. FDR was calculated using the Benjamin-Hochberg procedure.

(B and C) List of significantly enriched pathways (B) and functions (C) found by IPA among 1,086 genes significantly different (FDR < 5%, at least 2-fold) between SLe^{X-Hi} and SLe^{X-Low} CD4^{+} T cells. N, number of genes significantly changed in the pathway; % up, percentage of genes expressed at higher levels in SLe^{X-Hi} compared with SLe^{X-Low} CD4^{+} T cells; Z, activation *Z* score of the pathway or function predicted by IPA based on the direction of changes and contribution of membership genes; Positive, activated; negative, inhibited in SLe^{X-Hi}.

(D and E) Genes differentially expressed (FDR < 5%) in $SLe^{X\text{-}Hi}$ compared with $SLe^{X\text{-}Low}$ $CD4^+$ T cells that belong to (D) leukocyte extravasation signaling or (E) NF-κB signaling. Red dots are genes expressed at higher levels in $SLe^{X\text{-}Hi}$ compared with $SLe^{X\text{-}Low}$ $CD4^+$ T cells, whereas blue dots are genes expressed at lower levels in $SLe^{X\text{-}Hi}$ compared with $SLe^{X\text{-}Low}$ $CD4^+$ T cells.

KEY RESOURCES TABLE

REAGENT or RESOURCESOURCE	SOURCE	IDENTIFIER
Antibodies		
CD3-BUV805 clone UCHT1	BD Biosciences	cat# 565515; RRID:AB_2739277
CD4-BB700 clone SK3	BD Biosciences	cat# 566392; RRID:AB_2744421
CD8-BUV496 clone RPA-T8	BD Biosciences	cat# 564804; RRID:AB_2744460
CD14-BV510 clone M5E2	Biolegend	cat# 301842; RRID:AB_2561946
CD19-BV510cloneHIB19	Biolegend	cat# 302242; RRID:AB_2561668
CD25-BUV737 clone 2A3	BD Biosciences	cat# 564385; RRID:AB_2744342
CD27-BV570 clone O323	Biolegend	cat# 302825; RRID:AB_11149686
CD38-BUV661 clone HIT2	BD Biosciences	cat# 565069; RRID:AB_2744377
CD45RA-BUV563 clone HI100	BD Biosciences	cat# 565702; RRID:AB_2744407
CD69-PE clone FN50	BD Biosciences	cat# 555531; RRID:AB_395916
CD95-BV711 clone DX2	Biolegend	cat# 305644; RRID:AB_2632623
CD127-BV480 clone HIL-7R-M21	BD Biosciences	cat# 566101
CCR4-PE-CF594 clone 1G1	BD Biosciences	cat# 565391; RRID:AB_2739215
CCR5-BV650 clone 3A9	BD Biosciences	cat# 564999; RRID:AB_2739037
CCR6-BV421 clone 11A9	BD Biosciences	cat# 562515; RRID:AB_11154229
CCR7-APC-Cy7 clone G043H7	Biolegend	cat# 353211; RRID:AB_10915272
CXCR3-AF700 clone G025H7	Biolegend	cat# 353731; RRID:AB_2563532
CXCR4-PE Cy5 clone 12G5	BD Biosciences	cat# 555975; RRID:AB_396268
CXCR5-BB515 clone RF8B2	BD Biosciences	cat# 564624; RRID:AB_2738871
HLA DR-BV605 clone G46-6	BD Biosciences	cat# 562845; RRID:AB_2744478
FoxP3-PE Cy7 clone 236A/E7	eBioscience	cat# 25-4777-42; RRID:AB_2573450)
Ki67-BUV395 clone B56BDBiosciencescat# 56	BD Biosciences	cat# 564071; RRID:AB_2738577
PD-1-BV785 clone EH12.2H7	Biolegend	cat# 329930; RRID:AB_2563443
SLe^X (CD15s)-AF647 clone CSLEX1	BD Biosciences	cat# 563526; RRID:AB_2738258
CLA-AF647 clone HECA-452	Biolegend	cat# 321309; RRID:AB_2563661
CD19-142Nd clone HIB19	Fluidigm	cat# 3142001; RRID: AB_2651155
CD8-146Nd clone RPAT8	Fluidigm	cat# 3146001B; RRID: AB_2687641
CD62L-153Eu clone DREG56	Fluidigm	cat# 3153004B; RRID: AB_2810245
TIGIT-154Sm clone MBSA43	Fluidigm	cat# 3154016B; RRID: NA
CCR7-159Tb clone G043H7	Fluidigm	cat# 3159003A; RRID: AB_2714155
CD27-167Er clone L128	Fluidigm	cat# 3167006B; RRID: AB_2811093
CD45RA-169Tm clone HI100	Fluidigm	cat# 3169008B; RRID: NA
CD3-170Er clone UCHT1	Fluidigm	cat# 3170001B; RRID: AB_2811085
CD4-174Yb clone SK3	Fluidigm	cat# 3174004B; RRID: AB_2687862
Human Survivin Antibody clone 91630	R&D Systems	cat# MAB886, RRID:AB_2243438
HIV-1 core antigen-FITC, clone KC57	Beckman Coulter	cat# 6604665, RRID:AB_1575987
Human Fucosyltransferase 7/FUT7 Antibody clone 795116	R&D Systems	cat# MAB64091
B4GALT5 polyclonal antibody	Novus	cat# NBP2-14882
GAPDH antibody, clone 14C10	Cell Signaling Technology	cat# 2118, RRID:AB_561053

REAGENT or RESOURCESOURCE	SOURCE	IDENTIFIER
Peroxidase AffiniPure Donkey Anti-Rabbit IgG (H+L)	Jackson ImmunoResearch	cat# 711–035-152, RRID:AB_10015282
FUT6 Polyclonal Antibody	Thermo Fisher	cat# PA5-96261, RRID:AB_2808063
Bacterial and Virus Strains		
dfHIV	Generously provided to us by Dr. Leonard Chavez at Vitalant Research Institute	N/A
HIV-1 1MB	The Virus and Reservoirs Core at Penn Center for AIDS Research	N/A
HIV-1 89.6	The Virus and Reservoirs Core at Penn Center for AIDS Research	N/A
HIV-1 DH12	The Virus and Reservoirs Core at Penn Center for AIDS Research	N/A
HIV-1 NL43	The Virus and Reservoirs Core at Penn Center for AIDS Research	N/A
Biological Samples		
$CD4^+$ T cells isolated from PBMC of HIV-infected antiretroviral therapy (ART)-suppressed individuals	External Quality Assurance Program Oversight Laboratory (EQAPOL)- Duke Human Vaccine Institute's Immunology and Virology Quality	N/A
$CD4^+$ T cells isolated from PBMC of HIV-infected ART-suppressed individuals	The Wistar Institute and Philadelphia FIGHT	N/A
PBMCs from HIV-infected viremic and ART-treated individuals	INER-CIENI (Mexico)	N/A
PBMC from healthy individuals	University of Pennsylvania Human Immunology Core	N/A
Normal mouse serum	Thermo Fisher	cat# 501121171
Normal rat serum	Thermo Fisher	cat# 10710C
Human serum	Sigma-Aldrich	cat# H4522-20ML
Chemicals, Peptides, and Recombinant Proteins		
RPMI1640 medium	Corning	cat# 10-040-CM
Penicillin-Streptomycin	GIBCO	cat# 15140163
Fetal Bovine Serum	GIBCO	cat# 10437028
Recombinant Human IL-2	Prepotech	cat# 200-20
Recombinant Human TNF-α	Prepotech	cat# 300-01A
cis-Diammineplatinum(II) dichloride	Sigma-Aldrich	cat# P4394-25MG
AOL-biotin conjugated	TCI America	cat# A26591 ML
APC Streptavidin	Biolegend	cat# 405207
Ulex Europaeus Agglutinin I (UEA I), Fluorescein	Vector Labs	cat# FL-1061-2
Critical Commercial Assays		
TaqMan Universal Master Mix II, with UNG	Applied Biosystems	cat# 4440038
TaqMan Copy Number Reference Assay, human, TERT	Applied Biosystems	cat# 4403316
TaqMan RNA-to-CT 1-Step Kit	Applied Biosystems	cat# 4392656
Human RPLP0 (Large Ribosomal Protein) Endogenous Control	Applied Biosystems	cat# 4310879E
Brilliant Stain Buffer Plus	BD BioSciences	cat# 566385
Fixation/Permeabilization Solution Kit	BD BioSciences	cat# 554714

REAGENT or RESOURCESOURCE	SOURCE	IDENTIFIER
Perm/Wash Buffer	BD BioSciences	cat# 554723
Blotting-Grade Blocker	BIO-RAD	cat# 1706404
Falcon 48-well Clear Flat Bottom TC-treated Cell Culture Plate	Corning	cat# 353230
Foxp3/Transcription Factor Staining Buffer Set	eBioscience	cat# 00-5523-00
Cell-ID 20-Plex Pd Barcoding Kit	Fluidigm	cat# 201060
CyFACS buffer	Fluidigm	cat# MB-008
Cell-IDTM DNA Intercalator-Ir	Fluidigm	cat# 201192A
Maxpar cell staining buffer	Fluidigm	cat# 201068
Maxpar PBS	Fluidigm	cat# 201058
Maxpar Cell Acquisition Solution	Fluidigm	cat# 201240
EQTM calibration beads	Fluidigm	cat# 201078
Cy®3 Mono 5-pack	GE Healthcare	cat# GEPA23001
Dynabeads Human T-Activator CD3/CD28 for T Cell Expansion and Activation	GIBCO	cat# 11131D
eBioscience Foxp3 / Transcription Factor Staining Buffer Se	Invitrogen	cat# 00-5523-00
LIVE/DEAD Fixable Violet Dead Cell Stain Kit, for 405 nm excitation	Invitrogen	cat# L34955
ProteoExtract Subcellular Proteome Extraction Kit	Merck	cat# 539790
DEAE-dextran	MilliporeSigma	cat# D-9885
Anti-rat kappa MicroBeads	Miltenyi Biotec	cat# 130-047-401
LS columns	Miltenyi Biotec	cat# 130-042-401
QuadroMACS Separator	Miltenyi Biotec	cat# 130-090-976
MACS MultiStand	Miltenyi Biotec	cat# 130-042-303
HIV Infectivity Enhancement Reagent	Miltenyi Biotec	cat# 130-095-093
NEBNext Ultra RNA Library Prep Kit for Illumina	New England Biolabs	cat# E7530S
Bright-Glo Luciferase Assay System	Promega	cat# E2610
AllPrep DNA/RNA/miRNA Universal Kit	QIAGEN	cat# 80224
RNase-Free DNase Set	QIAGEN	cat# 79254
Bovine Serum Albumin	R&D Systems	cat# 5217
CyFACS buffer	Rockland	cat# MB-008
EasySep Human $CD4_+$ T Cell Isolation Kit	Stem Cell	cat# 17952
NuPAGE 4-12% Bis-Tris Protein Gels, 1.0 mm, 12-well	Thermo Fisher	cat# NP0322BOX
NuPAGE Sample Reducing Agent (10X)	Thermo Fisher	cat# NP0004
NuPAGE LDS Sample Buffer (4X)	Thermo Fisher	cat# NP0007
iBlot 2 Transfer Stacks, nitrocellulose, mini	Thermo Fisher	cat# IB23002
Novex Sharp Pre-stained Protein Standard	Thermo Fisher	cat# LC5800
SuperSignal West Pico PLUS Chemiluminescent Substrate	Thermo Fisher	cat# 34580
RIPA Lysis and Extraction Buffer	Thermo Fisher	cat# 89900
Bicinchoninic acid (BCA) assay	Thermo Fisher	cat# 23235
Halt Protease Inhibitor Cocktail (100X)	Thermo Fisher	cat# 87786
CL-XPosure Film, 8 × 10 in. (20 × 25 cm)	Thermo Fisher	cat# 34091
Deposited Data		

REAGENT or RESOURCESOURCE	SOURCE	IDENTIFIER
RNaseq data	Deposited to GEO (https://www.ncbi.nlm.nih.gov/geo/)	Accession number GSE151453
Experimental Models: Cell Lines		
ACH-2	NIH AIDS Reagent Program	cat# 349
H9	NIH AIDS Reagent Program	cat# 87
TZM-bl	NIH AIDS Reagent Program	cat# 8129
Oligonucleotides		
F522-43 (5′ GCC TCA ATA AAG CTT GCC TTGA3′	IDT	(Kumar et al., 2007)
R626-43 (5′ GGG CGC CAC TGC TAG AGA3′	IDT	(Kumar et al., 2007)
FAM-BQ probe (5′ CCA GAG TCA CAC AAC AGA CGG GCA CA 3′	IDT	(Kumar et al., 2007)
Software and Algorithms		
FlowJo software (Tree Star).	https://www.flowjo.com/	RRID:SCR_008520
bowtie2	http://bowtie-bio.sourceforge.net/index.shtml	RRID:SCR_005476
RSEM v1.2.12	http://deweylab.biostat.wisc.edu/rsem/	RRID:SCR_013027
DESeq2	https://bioconductor.org/packages/release/bioc/html/DESeq2.html	RRID:SCR_015687
QIAGEN's Ingenuity® Pathway Analysis software	https://digitalinsights.qiagen.com/	RRID:SCR_008653
Prism 6.0 and 7.0	http://www.graphpad.com/	RRID:SCR_002798
Rstudio	https://rstudio.com/	RRID:SCR_000432
FACSDiva software	http://www.bdbiosciences.com/instruments/software/facsdiva/index.jsp	RRID:SCR_001456
HiSeq control software	https://www.illumina.com/systems/sequencing-platforms/hiseq-2500/products-services/hiseq-control-software.html	N/A